LA-11414-MS
C.3

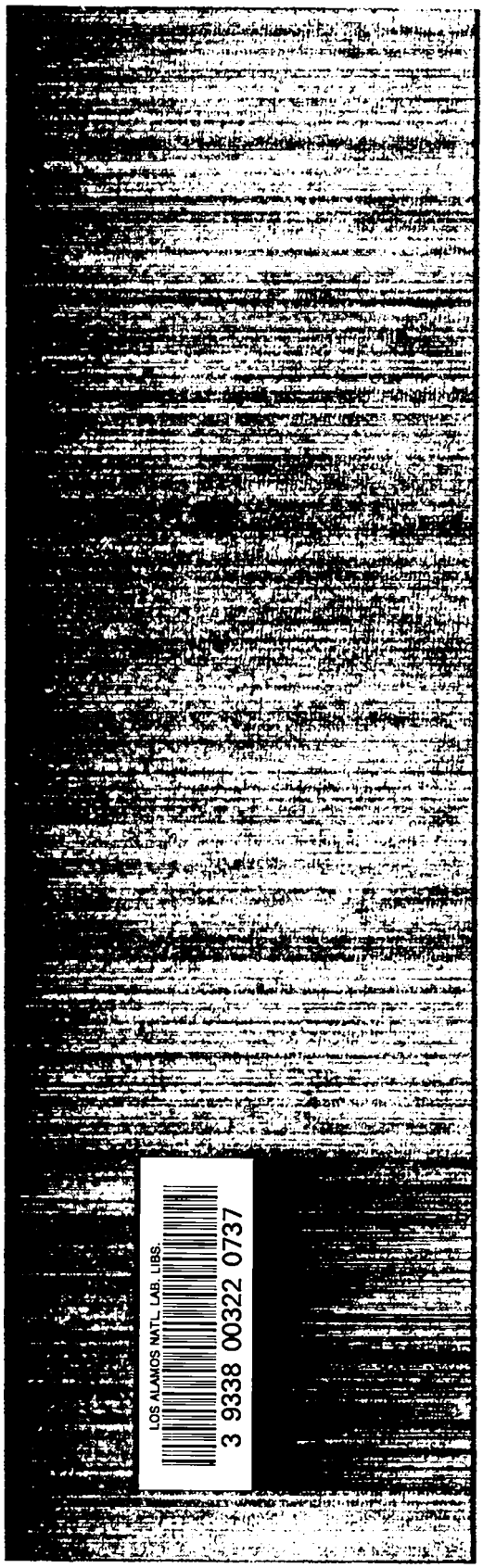

Measurements of Detonation-Wave Spreading and Local Particle Velocity at the Surface of 17-mm LX-07 Hemispherical Boosters

Los Alamos

Los Alamos National Laboratory is operated by the University of California for the United States Department of Energy under contract W-7405-ENG-36.

Prepared by Mary Ann Garcia, Group M-9

An Affirmative Action/Equal Opportunity Employer

LA-11414-MS

UC-741
Issued: December 1988

Measurements of Detonation-Wave Spreading and Local Particle Velocity at the Surface of 17-mm LX-07 Hemispherical Boosters

John C. Dallman

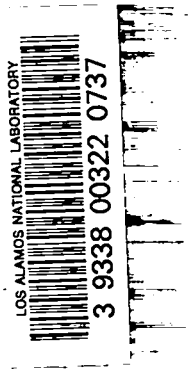

Los Alamos National Laboratory
Los Alamos, New Mexico 87545

MEASUREMENTS OF DETONATION-WAVE SPREADING AND LOCAL PARTICLE VELOCITY AT THE SURFACE OF 17-mm LX-07 HEMISPHERICAL BOOSTERS

by

John C. Dallman

ABSTRACT

The performance of the 17-mm hemispherical LX-07 explosive booster pellet is examined. Measurements are presented of the excess transit time, the emergence angle of the detonation wave, the velocity of an interface between the surface of the hemispherical pellet and a PMMA window at angles from 0° to 76° from the pole. Measurements are also presented, for a limited number of cases, of the shock velocities in the PMMA window that provide corroborative information about the detonation wave emergence angle.

I. INTRODUCTION

Hemispherical booster systems consisting of a hemisphere of explosive with an embedded detonator are used as part of an initiation train to smoothly initiate acceptor explosives that would be difficult or impossible to initiate with a simple detonator. Of particular interest for this study are the hemispherical booster systems used in the Los Alamos onion-skin test. This test measures the ability of an explosive to propagate a divergent detonation wave without the formation of regions of poor initiation or significant "dead zones" (no chemical reaction of the explosive). A schematic of a typical Los Alamos onion-skin test for PBX 9502 (95% 1,3,5-Triamino-2,4,6-Trinitrobenzene (TATB), 5% Kel-F 800, density 1.89 g/cm^3) is shown in Fig. 1. This test consists of a 1E34 detonator with a hemispherical LX-07 booster pellet (90% HMX, 10% Viton A, density 1.86 g/cm^3) joined to a hemispherical shell main charge through a glue joint

(typically Urethane 7200). Because it has been shown to be a size that readily differentiates manufacturing batch differences of PBX 9502 in the onion-skin test, the LX-07 booster size of interest in this study is a 17-mm-diameter hemisphere. In the performance of this experimental study only standard assembly techniques and tolerances were used with no special attempt made at improvement. These tests were performed at -54°C. A general study of the effect of booster dimensions, composition and temperature on the initiation and propagation of detonations in various TATB based explosives can be found in Ref. 1.

Although sensitivity to batch differences is the purpose of the onion-skin test, the rather large variations between batches of PBX 9502 using the 17-mm LX-07 hemispherical boosting system is of significant concern. This sensitivity may be due to uncontrolled properties of the booster system rather than solely due to inherent properties of the acceptor explosive. This report focusses on certain dynamic flow parameters of the boosting system and their reproducibility. Measurements are reported of the excess transit time, the emergence angle of the detonation wave at the pellet surface, as well as measurements of the particle velocity (pressure) at the interface between the pellet surface and an aluminized PMMA window. As a means of quantitative comparison the interface-velocity measurements are compared with the predictions of the Chapman-Jouguet theory at the explosive-PMMA interface.

II. DESCRIPTION OF THE EXPERIMENTS

A. Wave-Emergence Measurements

The LX-07 hemispherical pellets used in this study were pressed into the shape of a cylinder and then subsequently machined to the exact dimensions. The pellet densities were 1.860 ± 0.005 g/cm^3. A schematic of the pellet design is shown in Fig. 2. The outside diameter is 17.00 ± 0.16 mm. Located on center at the equator of the hemisphere

is a counterbore, for detonator insertion, with a diameter of 7.72 ± 0.05 mm. The typical detonator (1E34) used with the pellet has a 7.6-mm diameter. The dynamic tests were all performed at -54°C.

The first measurements on the performance of the detonator-pellet system were exactly the same as those done in the standard onion-skin test, that is, a measurement of the time of arrival of the detonation wave as a function of position at the hemisphere surface. The time of wave emergence at the pellet surface was referenced to the breakout of the shock wave at the surface of a fiducial detonator. For effective time analysis the fiducial detonator is identical in manufacture to the initiating detonator. A schematic of the wave emergence experimental configuration is shown in Fig. 3. Both detonators are initiated simultaneously by the firing circuit. A salt (aluminum silicofluoride, $Al_2(SiF_6)$), which emits light when it is strongly shocked, is painted on the surface of the hemisphere and the fiducial detonator. Two 45° mirrors provide enhanced visibility of the hemispherical pellet surface at large angles from the pole. The image of the hemisphere, the 45° mirrors, and the fiducial detonator are focussed on a 50-μm smear-camera slit, and the emitted light is recorded for analysis by the camera on photographic film.

Raw emergence data from four experiments are shown in Fig. 4. The time resolution in these records was about 6.5 ns for 12057 and 12058 and about 4.0 ns for 12059 and 12060. These measurements are shown as emergence time as a function of position with the pole of the hemisphere indicated by a vertical chain-dash line. These data are also presented as breakout time versus angle from the pole in Figs. A1 through A4 of Appendix A. As seen in Fig. 4 there is significant variation from side to side of the pellet. Although there appears to be a systematic lag of one side of the pellet over the other, there is no systematic azimuthal position of the hemispheres. The number of tests performed does not provide significant statistical information, but it does serve as

an indication of the variation from pellet to pellet. As will be shown later, the normal to the detonation wave for the four available studies makes only a very small angle ($\leq 1.0°$) with the normal to the surface of the pellet.

B. Velocimetry Measurements

The nearly perpendicular approach of the local normal to the detonation wave to the local surface tangent of the hemisphere indicates that it is not oblique impact of the shock wave with the acceptor interface that may cause poor initiation. Another possibility was that the pressure in the wave at large angles from the pole was down significantly. Hence, followed a natural extension of this study to the measurement of the variation of the velocity of an interface (pressure) between the explosive and a polymethylmethacrylate (PMMA) window over the surface of the booster pellet. The velocity measurement was done using a laser doppler velocimetry (LDV) technique (described below). A schematic of the experiment design is shown in Fig. 5. A PMMA disk with one surface having a hemispherical bore with the same radius of curvature as the pellet is glued to the pellet surface. The surface of the PMMA window in contact with the pellet surface has a vapor-deposited coating of $1.5 \cdot 10^{-2}$-mm-thick aluminum. The aluminized surface is in intimate contact with the surface of the hemispherical pellet through a glue junction (Eastman 910). This window was carefully attached at various angles from the pole, nominally 0°,.45°, 60° and greater. This angle was carefully measured using an optical comparator.

A schematic of a Fabry-Perot laser interferometric velocimeter is shown in Fig. 6. A more complete description of the design of this system is contained in Ref. 2. This system consists of a high-power argon ion laser operating single mode, a lens that is used both to focus the laser beam on target and to collect the diffusely scattered light from the target. The collected light from the target is then directed to the Fabry-Perot

interferometer producing a fringe pattern that is imaged on the slit of a rotating-mirror image-intensified streak camera. A cylindrical lens is used in front of the interferometer to produce sufficient convergence of the beam to give the desired number of fringes. This system uses an extremely sensitive technique (the interferometer) to measure the doppler shift of the scattered light from a moving target. From the measurement of the doppler shift of the scattered light the velocity of the target can be determined. A complete description of the analysis of Fabry-Perot interferometric data is outside the scope of this report. However, relevant descriptions of the analysis of doppler shift measurements with the Fabry-Perot interferometer are contained in Refs. 2, 3, and 4. The time resolution of the velocity measurements was approximately 5 ns. The resolution in velocity varied since it is somewhat dependent on quality of exposure. However, the error in the velocity measurement was generally less than ± 2.0%.

III. PREDICTION OF THE SIMPLEST THEORY

The purpose of this section is to provide theoretical calculations of the flow parameters that will create a backdrop against which to compare the experimental measurements. The goal is to calculate the interface velocity between the explosive and the PMMA window. Although the system of interest, see Fig. 5, is not a simple one-dimensional system, the reaction zone of LX-07 is very small compared to the size of the experiment. This provides some confidence that a simple theory[5] such as the Chapman-Jouguet theory can provide quantitative information against which to compare the experimental results of this study. The theory assumes that the flow is one dimensional, that all reaction takes place instantaneously with the detonation front represented as a jump discontinuity, that the propagation of this discontinuity is steady, that we have reasonable equations of state for the explosive and the receptor inert, and

that the discontinuity propagates with the unique velocity of the Chapman-Jouguet point.

The conservation laws can be written as

$$\text{Mass} \qquad (D - U_p)\rho = \rho_0 D \tag{1}$$

$$\text{Momentum} \qquad P = \rho_o D U_p \tag{2}$$

$$\text{Energy} \qquad E + P/\rho + (U_p - D)^2/2 = D^2/2 \tag{3}$$

where U_p is the particle velocity in the laboratory, D is the shock front velocity, ρ is the density of the shocked material, ρ_0 is the initial density of the explosive, P the pressure and E the specific internal energy.

An approximate equation of state for the explosive product gases is the polytropic gas equation of state with constant heat capacity for a Chapman-Jouguet explosive

$$E = P/((\gamma - 1)\rho) - q \tag{4}$$

where $D_{CJ}^2 = 2(\gamma^2 - 1)q$, q is the total heat of reaction and $\gamma = -\frac{\partial \ell n p}{\partial \ell n v}|_s$ is the negative logarithmic slope of the isentrope. And the equation of state for the PMMA can be represented by a linear relation between the shock velocity and the particle velocity, $U = C_o + SU_p$ with the values for the constants obtained from Ref. 6.

Solving these equations in the usual manner using the reflected Hugoniot as an approximation to the isentrope and with P_{CJ} = 34.6 GPa (Ref. 7) and D_{C_J} = 8.64 mm/μs for LX-07, the calculated particle velocity at the explosive-PMMA interface is 2.92 mm/μs. This is the velocity against which the measured interface velocities of the following section will be compared.

IV. DISCUSSION OF THE DATA

A. Shock-Wave Emergence Data at the Pellet Surface

1. Isotropy

Measurements of the detonation-wave emergence at the surface of the pellet are compared in Fig. 4. These tests show a side-to-side variation of first breakout in the same test from a few nanoseconds (at or below the limit of resolution of the measurements) to about 21 ns over the four experiments, and a maximum of 58 ns difference between first breakout and breakout at the pole.

Figure 2 indicates the tolerances involved in the fabrication of the pellet. The exact position of the 7.6-mm-diameter detonator in the counterbore along with the other tolerances, to a first order approximation, appear to be sufficient to account for the side-to-side differences in breakout time. To put these variations in perspective, differences of 21 ns represent spatial differences (if detonation velocity is fully attained) of about 0.18 mm. That is, the detonation wave at one side trails about 0.18 mm behind the other. Thus the small differences involved with positioning of the detonator in the counterbore and other tolerances can account for most of the observed variation.

2. Initiation

An indication of the approach of a dynamic explosive system to that of a steady state system can be measured by comparing the wave transit time in the actual system to that of an ideal system. An excess transit time can be defined as

$$t_{\text{excess}} = t_{\text{breakout}} - d/D \tag{5}$$

where d is the distance the detonation wave travels and D is the infinite medium detonation velocity. This type of calculation assumes that the divergent wave velocity will be very close to the infinite medium velocity. This assumption is probably very good

near the pole, but less good at large angles from the pole. A maximum excess transit time of 34 ns was measured at the pole. However, Figs. 7, 8, 9, and 10 show a continuous calculation of the estimated excess transit time over the entire surface of the pellet. The excess transit times at large angles from the pole can be as much as a factor of ten greater than at the pole. These large excess transit times indicate that this system may not be at a steady condition (i.e. the detonation is accelerating) over much of the radial propagation of the detonation and may never attain the infinite medium velocity.

B. Shock-Emergence Angle at the Pellet Surface

The wave-breakout data provide the time and position of the emerging detonation wave from the hemispherical surface. However, given these data as an initial value the angle formed by the normal to the detonation wave with the normal of the pellet surface can be obtained using a Huygen's construction with an 8^{th} degree polynomial fitted to the measured data.[8] An assumption required is that the detonation wave velocity in the direction normal to its surface is not accelerating strongly in the neighborhood of the surface. The value of the velocity used was $D = 8.64$ mm/μs, the infinite-media detonation velocity. With these assumptions Figs. 11, 12, 13, and 14 show the emergence angle as a function of radial angle at the surface of the hemisphere. Over the region of radial angle 0 to 80° the emergence angle for the four tests is less than about 0.1°. This is a very small angle, but it should be recognized that small changes in any of the above assumptions will result in some variation from these values (although velocities less than the infinite-media detonation velocity would result in smaller angles not larger).

C. Particle Velocity at the Pellet-Window Interface

The results of the emergence-angle analysis prompted an extension of this study to the study of the particle velocity at an interface between the explosive and a PMMA window. A table of the parameters of all the velocimetry experiments as well as the

analyzed velocity-history data from the 20 velocimetry studies are shown in Figs. B1 through B20 of Appendix B. The time histories after the jump or initial velocity are subject to "error" because the interferometer is receiving light that has passed through a radially diverging shock front.[4] The error is cumulative and can be significant at long times. This "error" can be corrected if certain assumptions are made about the hydrodynamic properties of the flow. However, at early times (< 0.1 μs) the error is small, and it was ignored in the analysis that follows.

There is considerable variation in the exact shape of the velocity histories. The source of this variation is not completely understood, but a dominant cause must certainly be differences in the early initiation of the explosive that propagate to the surface of the hemisphere. Therefore, a good choice for a point of comparison among the various experiments is the jump velocity, the interface velocity at the instant the shock wave reaches the PMMA window, since it does not suffer from the problems of the shock in the window material nor those of long time variations.

Because the jump velocity can be strongly influenced by the first few exposed grains of photographic emulsion on the record, it was decided to fit the velocity-time data with an empirical fit of the form

$$V(t) = A + Bt + Ce^{-Dt} \quad . \tag{6}$$

This form has been used by other investigators[9] with good results, and thus it was considered a reasonable choice. In order to minimize problems caused by the shocked window material, this form was fit over the first 0.10 μs of the time history. The fit was applied in a standard nonlinear least squares sense and the value of the form at $t = 0$ was used as the jump velocity.

The calculated jump velocities are shown in Fig. 15 as a function of the angle measured from the pole of the hemisphere. The velocities appear fairly constant out

to about 65°. The measurements of the jump velocity at 75° show a drop to about 8% below the predicted value of 2.92 mm/μs. Using a model of the detonation that involved slow-time scale shock dynamics of the explosive with a completely time-resolved heat release, Bdzil and Stewart[10] have shown that the unsupported boundary in the pellet geometry begins to strongly influence the detonation wave dynamics at about 80° from the pole. In a qualitative sense, the data of this study appear to support this theoretical work. A comparison with the velocity calculated from the simple theory (2.92 mm/μs), represented by the straight line in Fig. 15, indicates that the measured velocities compare quite well for angles less than 65°.

These data give some indication of why the 17-mm hemispherical pellet provides acceptor or test explosive batch discrimination in the onion-skin test. Certainly as the interface velocity (pressure) at large angles from the pole begins to drop, conditions become increasingly marginal for the initiation of the acceptor explosive in the test. Additionally, at very large angles the approach of the detonation wave begins to deviate from the perpendicular. Under these conditions, small differences in the properties of the acceptor may be amplified and become apparent at the surface of the acceptor explosive.

D. Shock Velocity in the PMMA Window

The velocity of the shock wave in the PMMA window was measured in only a few of the experiments. Since the shock wave separates regions of differing density there is a change in the index of refraction and the possibility of significant reflection from this interface. The reason, that these data are not available for all of the experiments, is that the reflection at this shock interface is only a few percent of the incoming light. Since the recording exposures for these experiments were set at a level to measure the

explosive-PMMA interface reflection, the few percent of reflected light from the shock interface was at or near the limits of the recording systems exposure requirements.

The measurement of the shock velocity in the PMMA window provides an indirect way to calculate the emergence angle of the detonation wave at the pellet surface. Figure 16 shows an idealization of the interaction of a shock wave at an interface between two dissimilar materials. The detonation or shock wave in Material I intersects the interface at an angle, θ. The normal direction of propagation of the resultant shock wave in Material II (the PMMA window in this case) makes an angle ω with the normal to the interface. Linear shock Hugoniot relations assume the velocities used in the relations are normal to the wave front. Using the terminology of Fig. 16, the normal velocity of the shock in Material II is

$$\vec{U}_s^{\perp} = D(\sin\omega/\sin\theta)\vec{n} \tag{7}$$

The linear Hugoniot relation can now be written

$$\vec{U}_s^{\perp} = C_0\vec{n} + S\vec{U}_p^{\perp} \tag{8}$$

The projection of this equation along j, the direction of LDV measurement,

$$\vec{U}_s^{\perp}\cdot\vec{j} = C_0\vec{n}\cdot\vec{j} + S\vec{U}_p^{\perp}\cdot\vec{j} \tag{9}$$

with $\vec{n}\cdot\vec{j} = \cos\omega$. Rewriting Eq. (9) as a scalar equation, it becomes

$$U_{\text{sobs}} = C_0\cos\omega + SU_{\text{pobs}} \tag{10}$$

where the "obs" subscript indicates the velocity observed by the LDV system. With values[6] of $C_0 = 2.598$ mm/μs and $S = 1.516$ the value of ω, the shock propagation angle, can be calculated using Eq. (10). Now

$$U_{\text{sobs}} = \vec{U}_s^{\perp}\cdot\vec{j} = D(\sin\omega/\sin\theta)\cos\omega \tag{11}$$

With the assumption that the value of D is known, θ, the angle the normal to the emergent shock wave makes with the normal to the pellet surface, can be obtained from Eq. (11).

The method of analysis of the histories for the shock velocities in the PMMA window is exactly the same as for the explosive-window interface. The point of comparison among the data sets is the shock jump velocity. The shock-velocity histories for the five available cases are shown in Figs. C1 to C5 of Appendix C. Table 1 shows a comparison of the measured shock velocities in the window and particle (interface) velocities along with the calculated angles of propagation of the shock in the window and the detonation wave emergence angle. Of the available five experiments where both shock and interface velocities were measured, the range of values for the emergence angles were from 0.29° to 14.0°. The shock-velocity data are far less reliable because the exposures tended to be rather poor, and there is some overlaying of the interface and shock fringes on the photographic record. In spite of this, these measurements give qualitative corroboration that the detonation wave emergence angles are small.

V. CONCLUSIONS

The basic conclusion of this study is that the 17-mm LX-07 hemispherical booster performs extremely well. The detonation wave appears to spread in a spherical manner from the detonator. This is supported by the measurements of the emergence angles, which over the entire pellet all measure less than 1.0°. Additionally, the calculated emergence angles based on the shock jump velocity measurements indicate small emergence angles for the detonation wave. With the emergence angle being small it was of interest to measure the particle velocity at the surface of the pellet. These measurements show a flat profile until angles from the pole greater than 75° are attained. At angles greater than 75°, a drop in the particle velocity at the PMMA window — explosive interface is

measured. Thus this region begins to show the influence of the unsupported equatorial region of the hemisphere, and gives some indication of why the LX-07 17-mm pellet in the PBX 9502 onion-skin test provides good sensitivity to possible batch mixture differences.

TABLE 1

TABLE OF CALCULATED SHOCK WAVE EMERGENCE ANGLES, θ, AND DETONATION WAVE EMERGENCE ANGLES, ω, FOR FIVE EXPERIMENTS WHERE BOTH THE INTERFACE VELOCITY AND THE SHOCK VELOCITY IN THE PMMA WINDOW WERE SIMULTANEOUSLY MEASURED

SHOT NO.	ANGLE FROM POLE Degrees	U_{pobs} mm/μs	U_{sobs} mm/μs	θ Degrees	ω Degrees
F1901	75.68	2.71	6.65	11.9	14.0
F1903	73.85	2.71	6.71	4.0	5.1
F8094	63.98	2.96	7.48	6.3	7.23
F8127	58.88	2.87	6.96	0.2	0.29
F8130	42.75	2.85	7.09	3.7	4.5

ACKNOWLEDGEMENTS

I would like to acknowledge the many insightful comments of John B. Bdzil, and his contributions involved in the checking and sometimes redoing of the calculations presented; the software and techniques developed by Charles A. Forest to fit hemispherical geometry wave breakout data and convert it to emergence angle; and the help and patience of the experimental firing site leader, Sandra H. Hildner. Additionally, experiments F1743, F1744, F1746, and F1747 were performed by George West, while on leave from Pantex, and Howard L. Stacy. And, finally to Wendell L. Seitz for suggesting and supporting this study.

REFERENCES

1. K. Bahl, G. Bloom, L. Erickson, R. Lee, C. Tarver, W. Von Holle, R. Weingart, "Initiation Studies on LX-17 Explosive." Eighth Symposium (International) on Detonation (NSWC MP 86-194, Silver Springs, MD, 1985), pp. 1045–1056.
2. W. L. Seitz, and H. L. Stacy, "Fabry-Perot Interferometry Using an Image-Intensified Rotating-Mirror Streak Camera," Proc. SPIE on High Speed Photography, Videography, and Photonics **427**, 186 (1983).
3. D. R. Goosman, "Measuring Velocities by Laser Doppler Interferometry," Energy and Tech. Rev., Lawrence Livermore Laboratory Report UCRL-52000-79-3 (1979).
4. J. Wackerle, H. L. Stacy, J. C. Dallman, "Refractive Index Effects for Shocked Windows in Interface Velocimetry," SPIE on High Speed Photography, Videography, and Photonics, 31st Annual Int. Tech. Symp., (1987).
5. W. Fickett, W. C. Davis, Detonation, (Univ. of California Press, Berkeley, 1979), pp. 13–42.
6. GMX-6 Data Base, "Selected Hugoniots," Los Alamos Scientific Laboratory Report LA-4167-MS (May 1969).
7. B. M. Dobratz, "LLNL Explosives Handbook," UCRL-52997 (March, 1981), pp. 19–73.
8. C. Forest, "Onion-Skin Data and Geometric Waves," Los Alamos Internal Report M-9-QR-87-1 (1987).
9. W. L. Seitz, H. L. Stacy, J. Wackerle, "Detonation Reaction Zone Studies on TATB Explosives," Eighth Symposium (International) on Detonation (NSWC MP 86-194, Silver Springs, MD, 1985), pp. 123–132.

10. J. B. Bdzil, D. S. Stewart, "Detonation Shock Dynamics: The Onion-Skin Geometry," Los Alamos Internal Report M-9-QR-86-3 (1986).

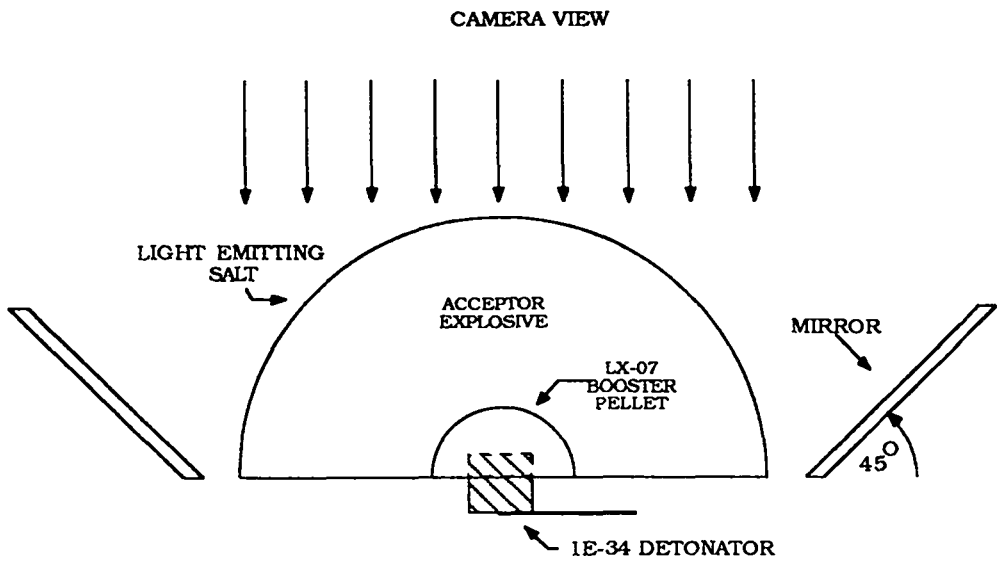

Fig. 1. Schematic of typical Los Alamos onion-skin test.

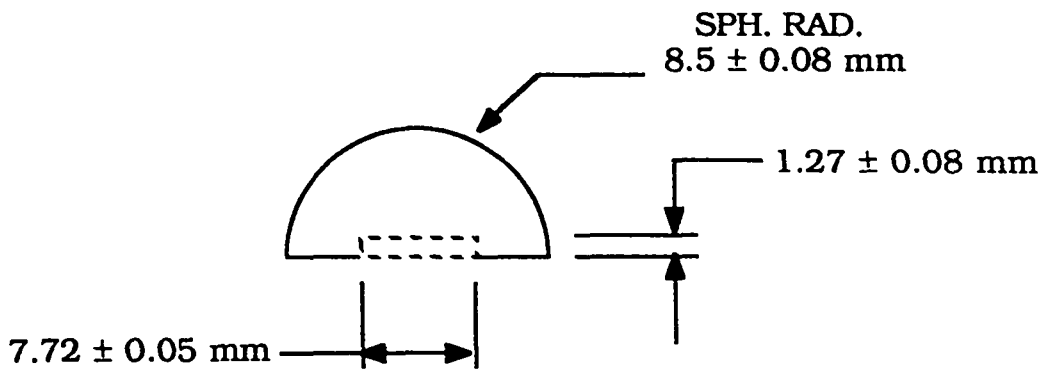

Fig. 2. Design parameters for the LX-07 hemispherical booster pellet.

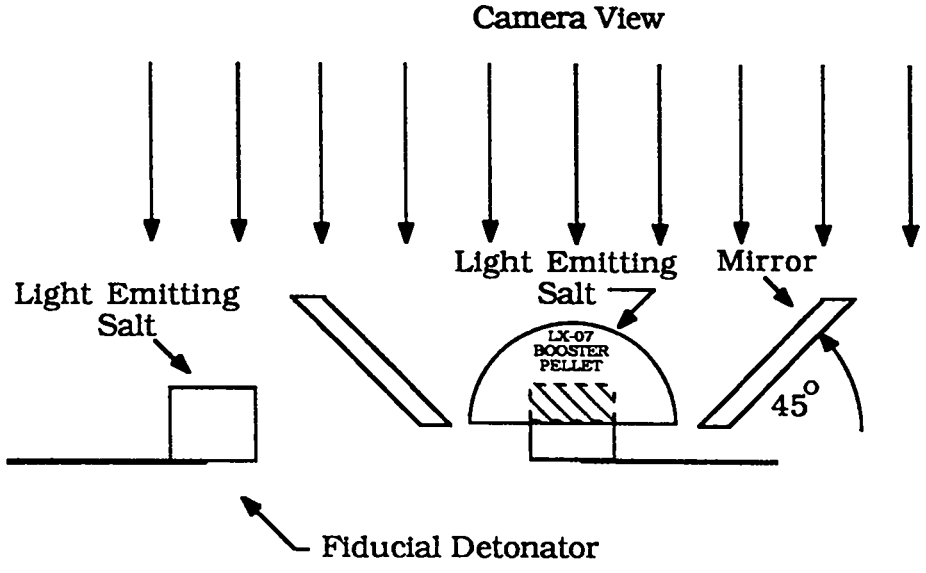

Fig. 3. Schematic of wave-emergence experiment for LX-07 17-mm hemispherical booster pellet.

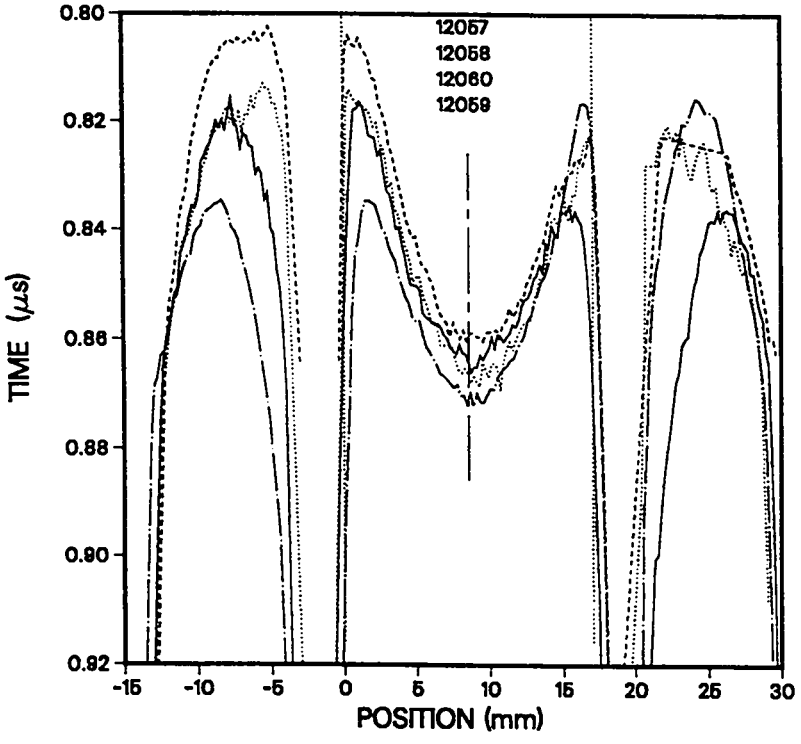

Fig. 4. Raw emergence data for the LX-07 booster pellet experiments. Vertical dotted lines represent pellet edges and vertical chain-dash line the pellet pole.

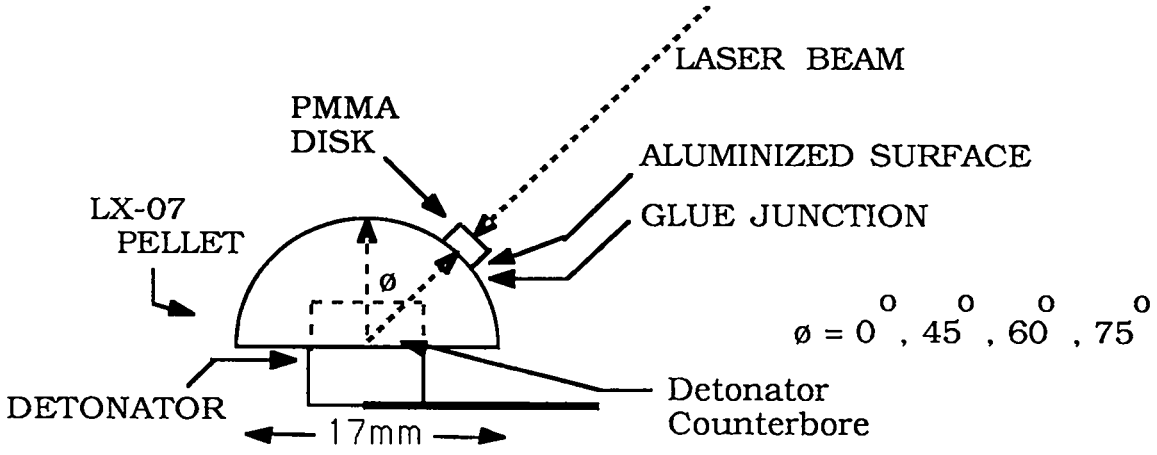

Fig. 5. Schematic of the velocity measurement experiments.

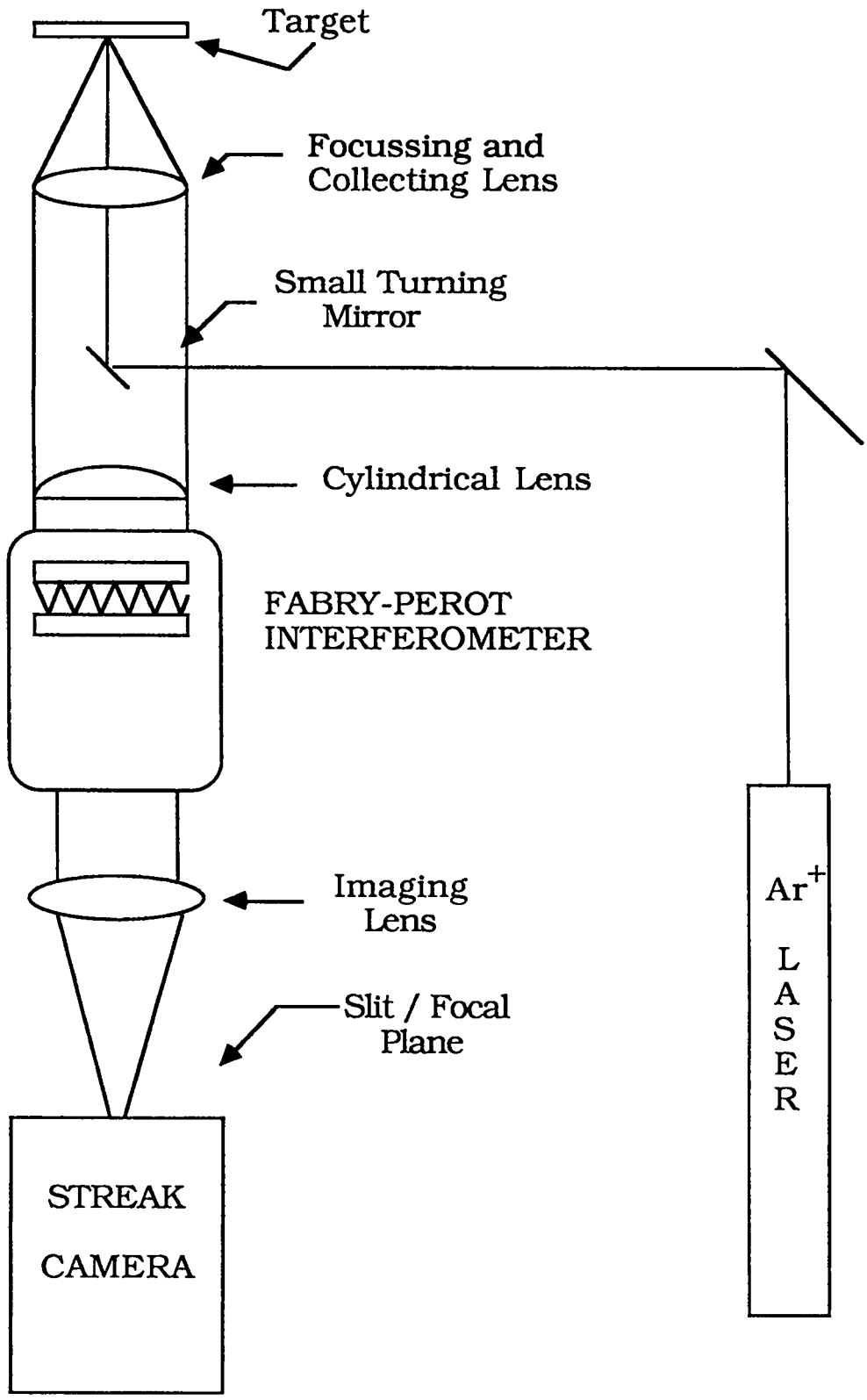

Fig. 6. Schematic of the LDV system.

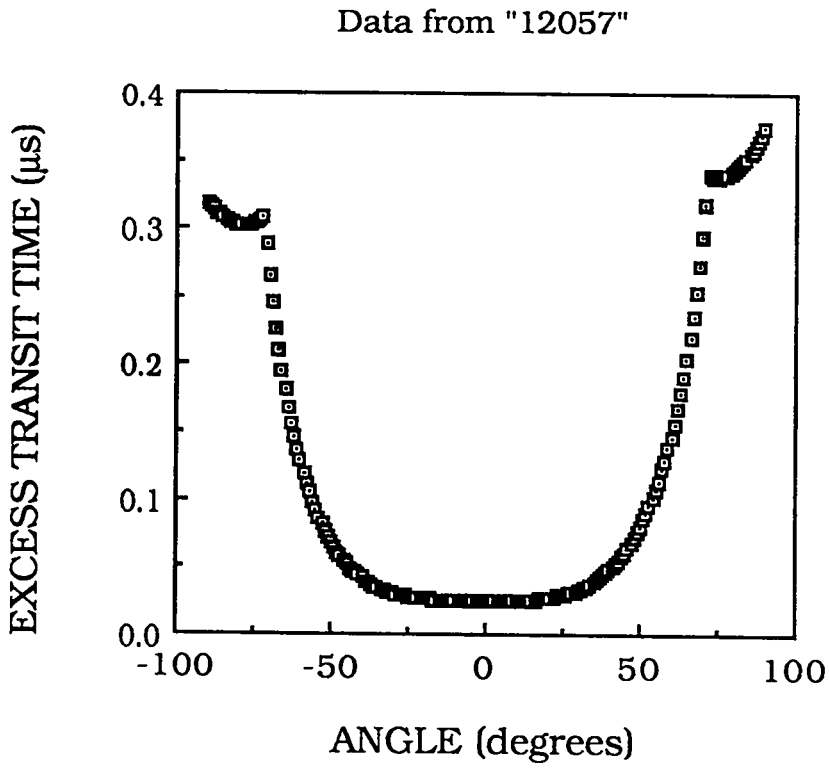

Fig. 7. Continuous excess transit time across the entire pellet for Shot Number 12057.

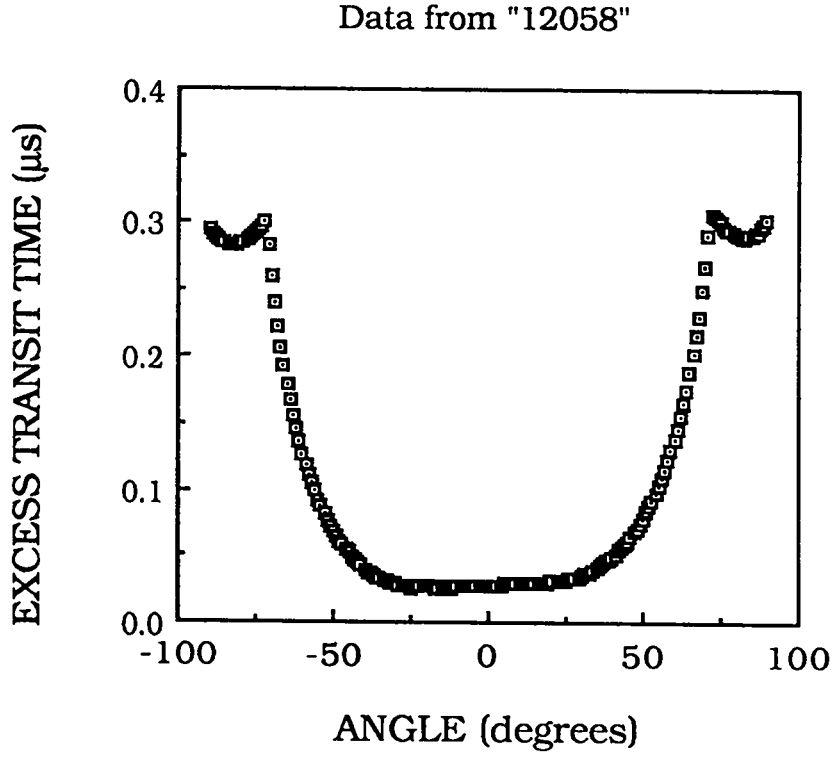

Fig. 8. Continuous excess transit time across the entire pellet for Shot Number 12058.

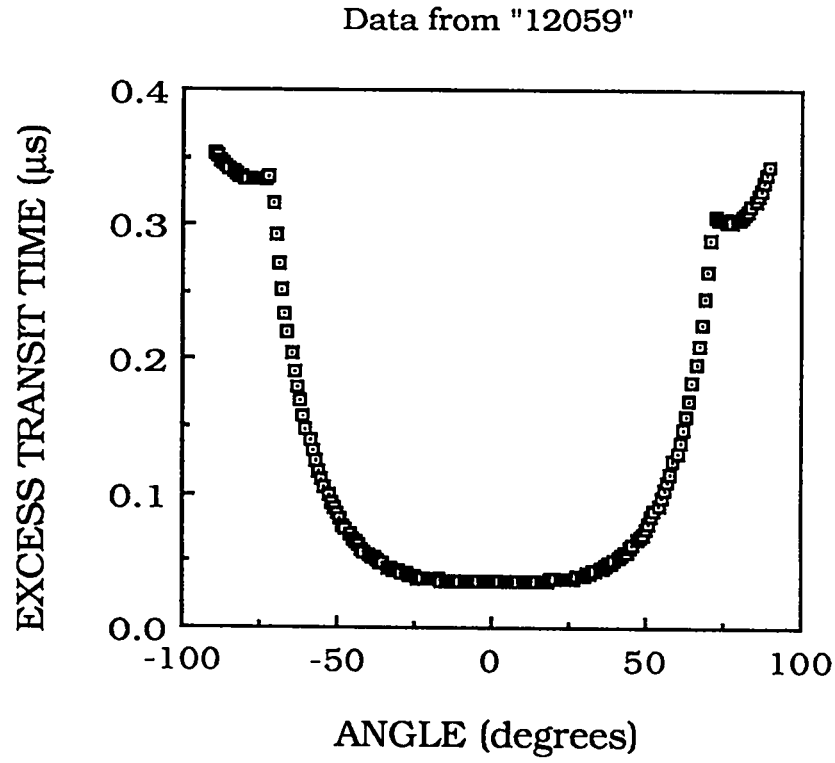

Fig. 9. Continuous excess transit time across the entire pellet for Shot Number 12059.

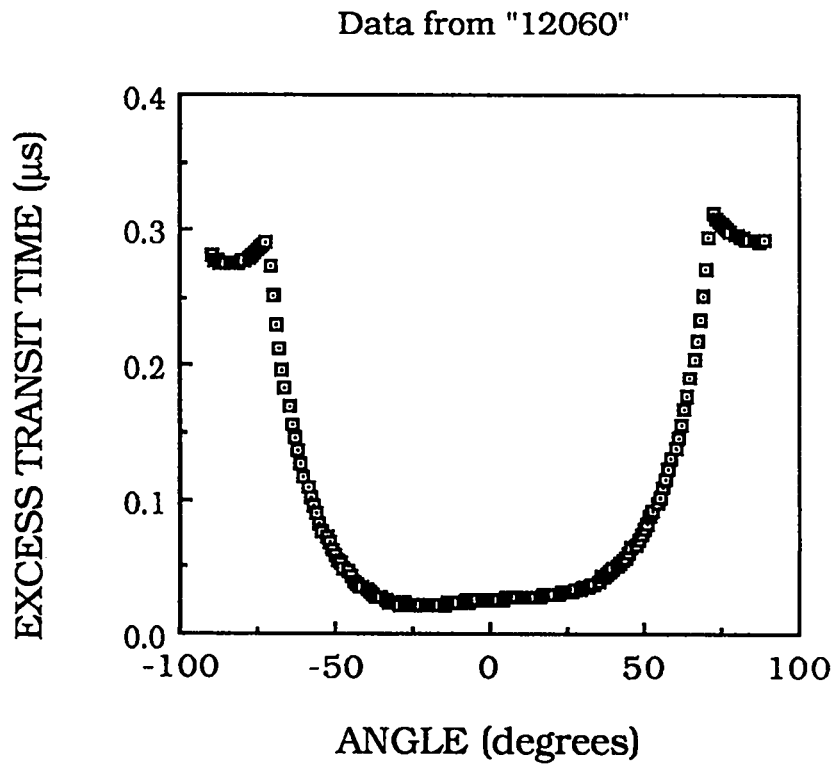

Fig. 10. Continuous excess transit time across the entire pellet for Shot Number 12060.

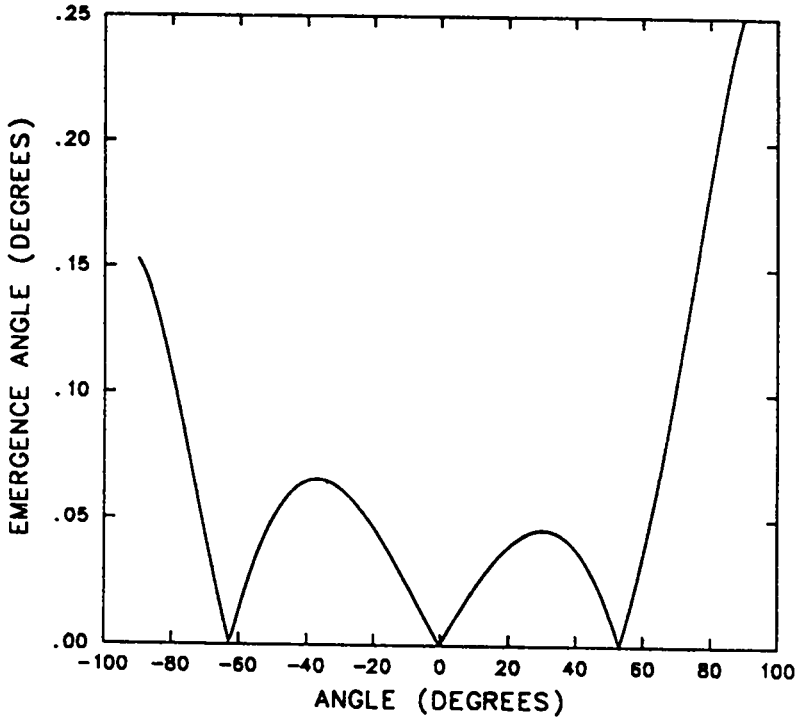

Fig. 11. Detonation-wave emergence angles for the LX-07 booster pellet. Shot Number 12057.

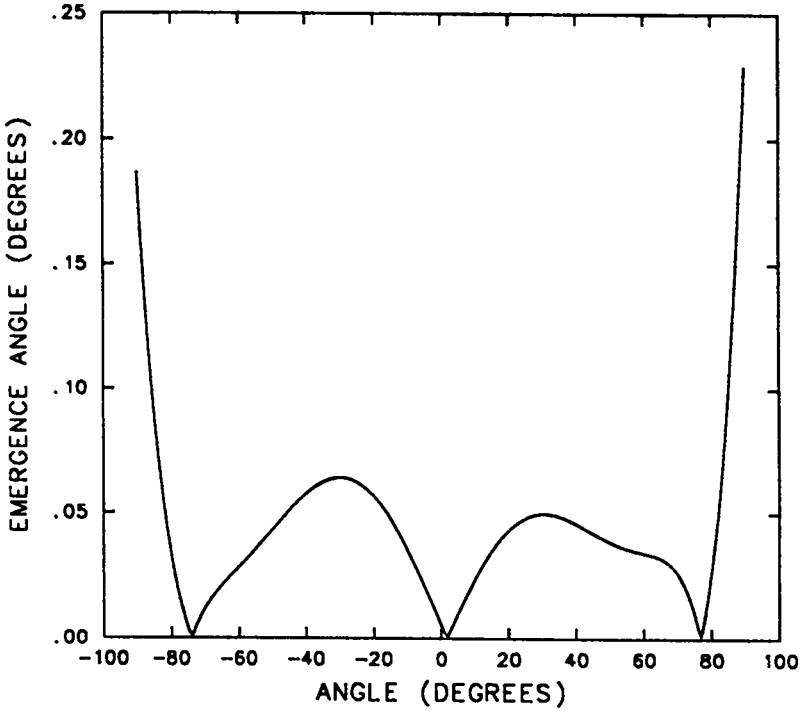

Fig. 12. Detonation-wave emergence angles for the LX-07 booster pellet. Shot Number 12058.

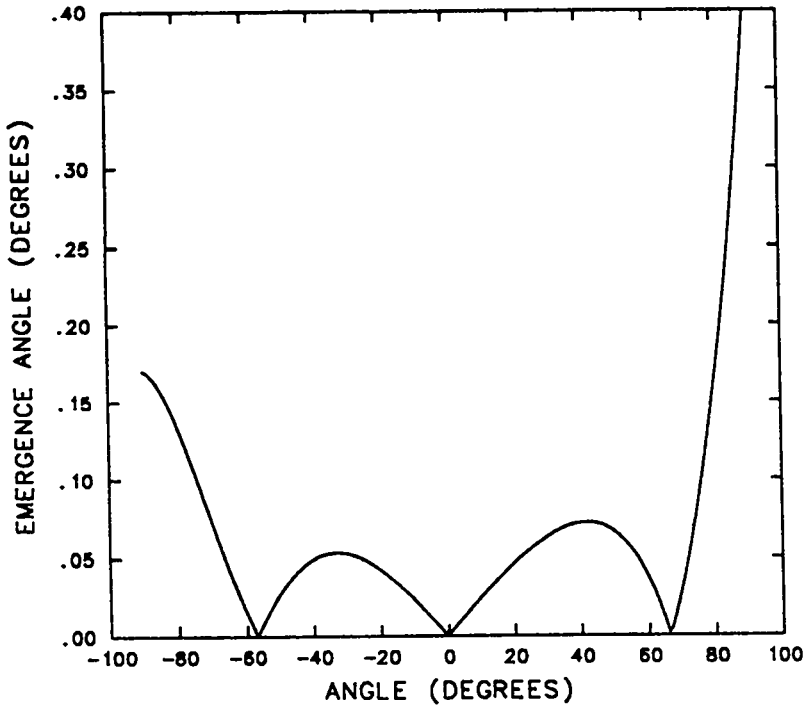

Fig. 13. Detonation-wave emergence angles for the LX-07 booster pellet. Shot Number 12059.

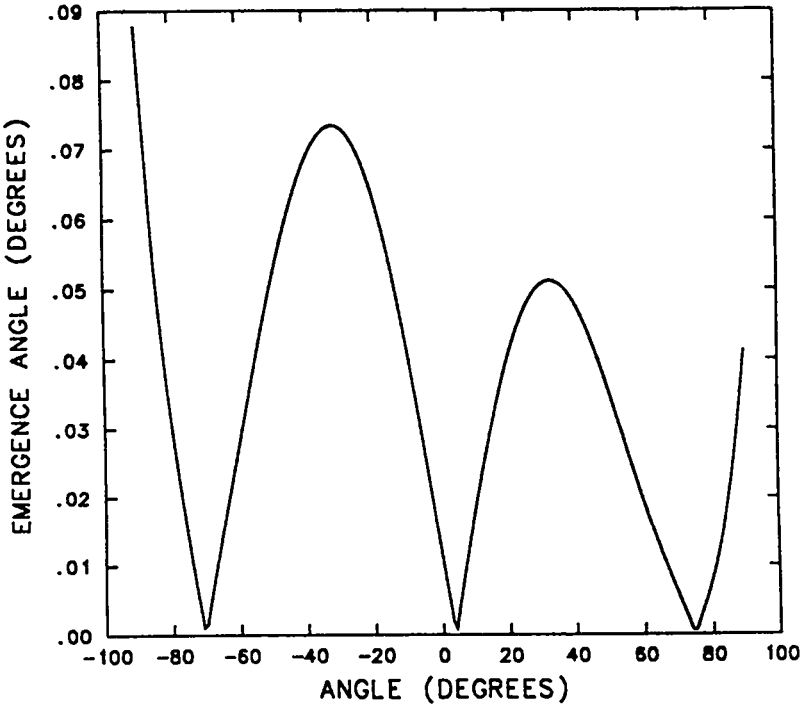

Fig. 14. Detonation-wave emergence angles for the LX-07 booster pellet. Shot Number 12060.

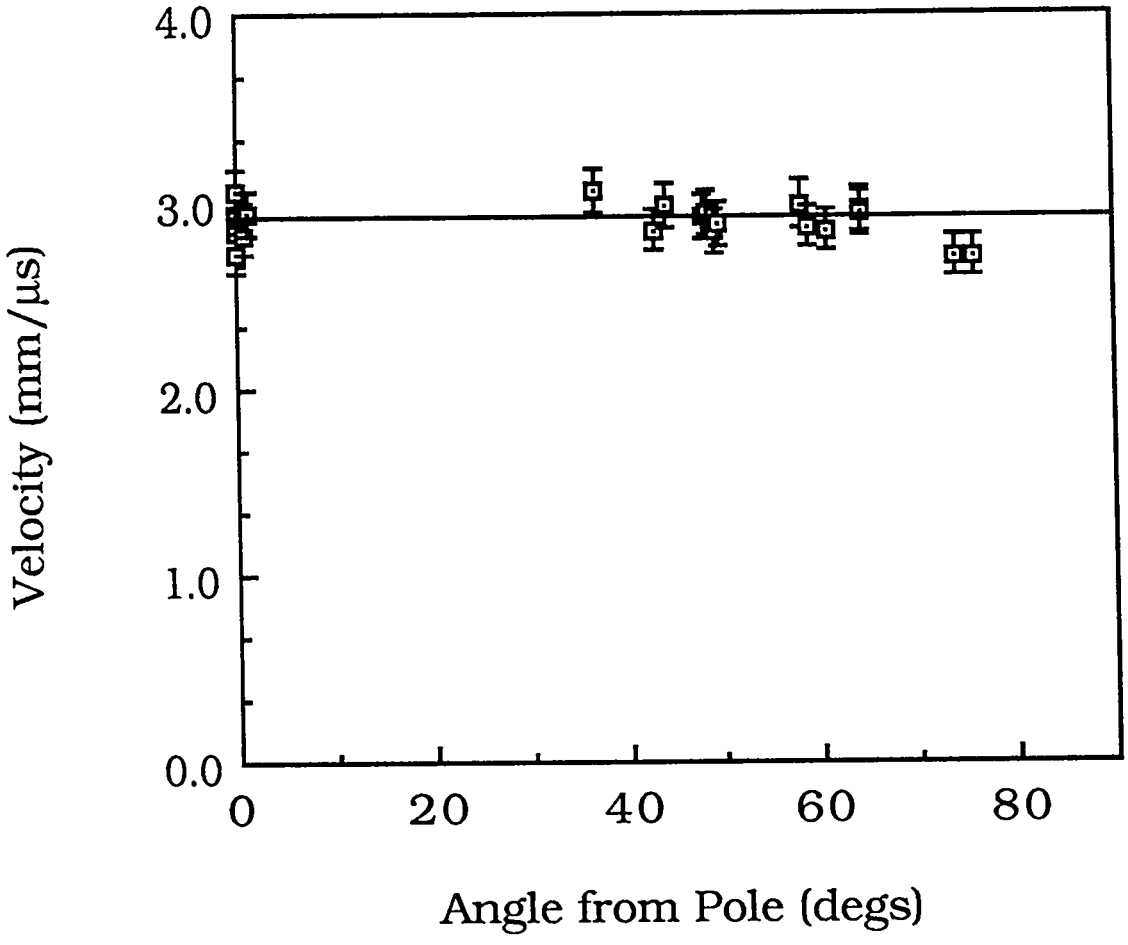

Fig. 15. Interface jump velocities for PMMA window 1 LX-07 pellet interface versus the radial angle from the hemisphere pole. Solid line represents the Chapman-Jouguet detonation model prediction.

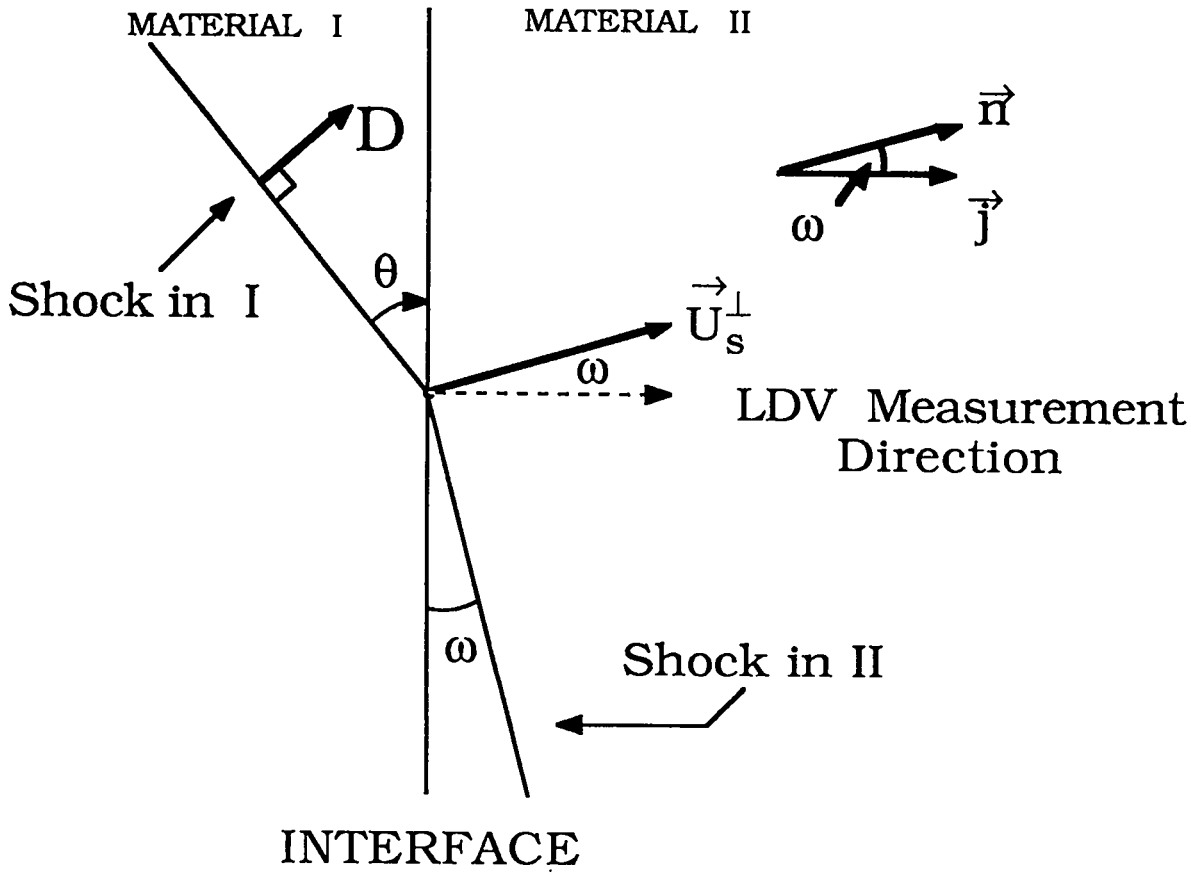

Fig. 16. Idealization of the interaction of a shock wave at the interface between two dissimilar materials.

APPENDIX A

WAVE EMERGENCE TIME VERSUS ANGLE FROM THE POLE FOR THE LX-07 HEMISPHERICAL PELLET

The symbols used in the figures of Appendix A can be interpreted in terms of Fig. 3. The open and filled squares are data from the left and right mirrors respectively. The filled diamonds are data recorded from direct viewing of the hemispherical surface.

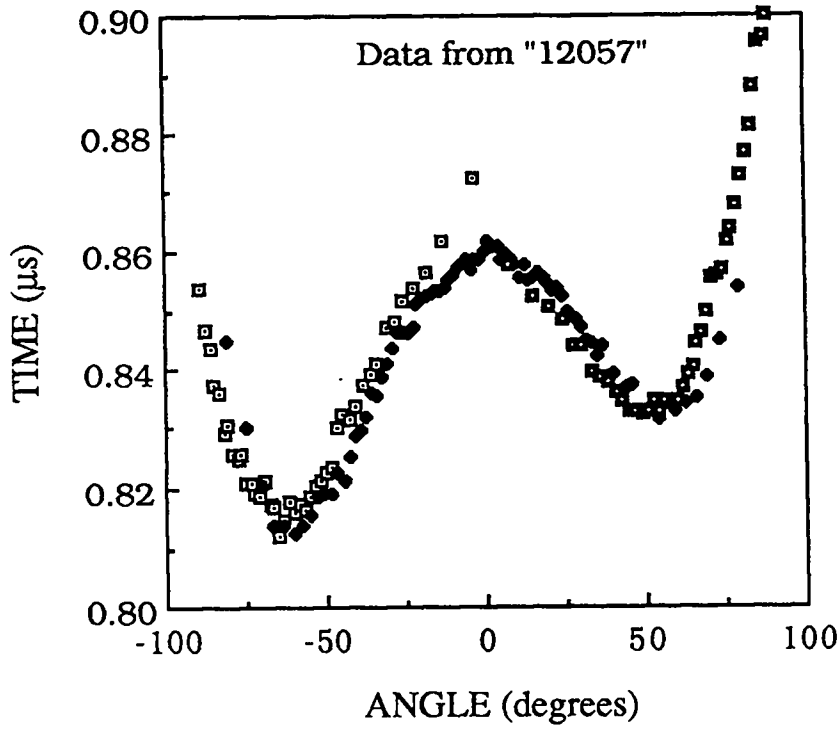
Data from "12057"
0.90
0.88
0.86
0.84
0.82
0.80
TIME (μs)
-100
-50
0
50
100
ANGLE (degrees)

A1

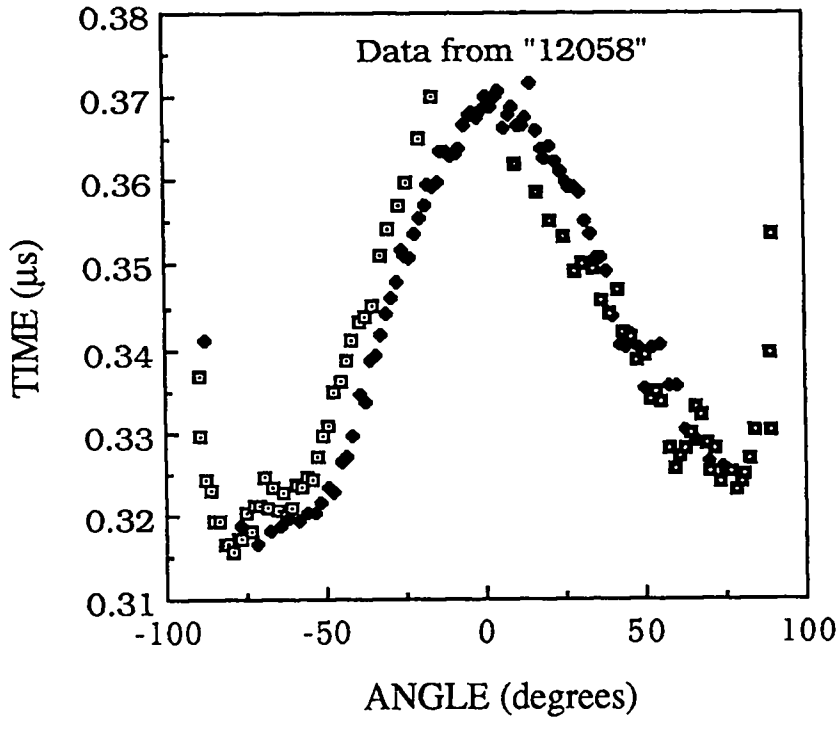
Data from "12058"
0.38
0.37
0.36
0.35
0.34
0.33
0.32
0.31
TIME (μs)
-100
-50
0
50
100
ANGLE (degrees)

A2

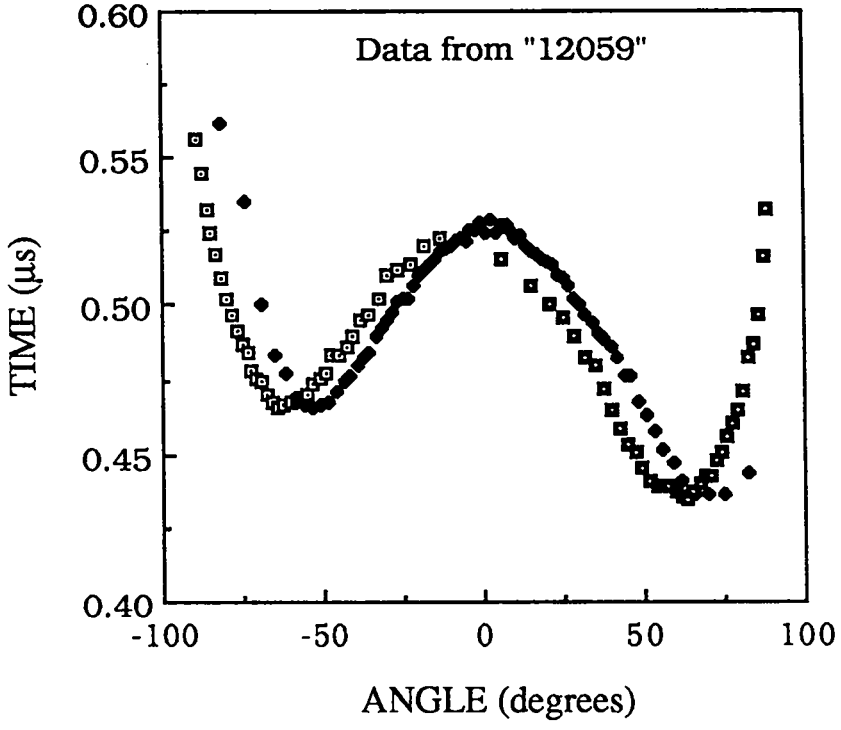
Data from "12059"
TIME (µs)
0.60
0.55
0.50
0.45
0.40
-100
-50
0
50
100
ANGLE (degrees)

A3

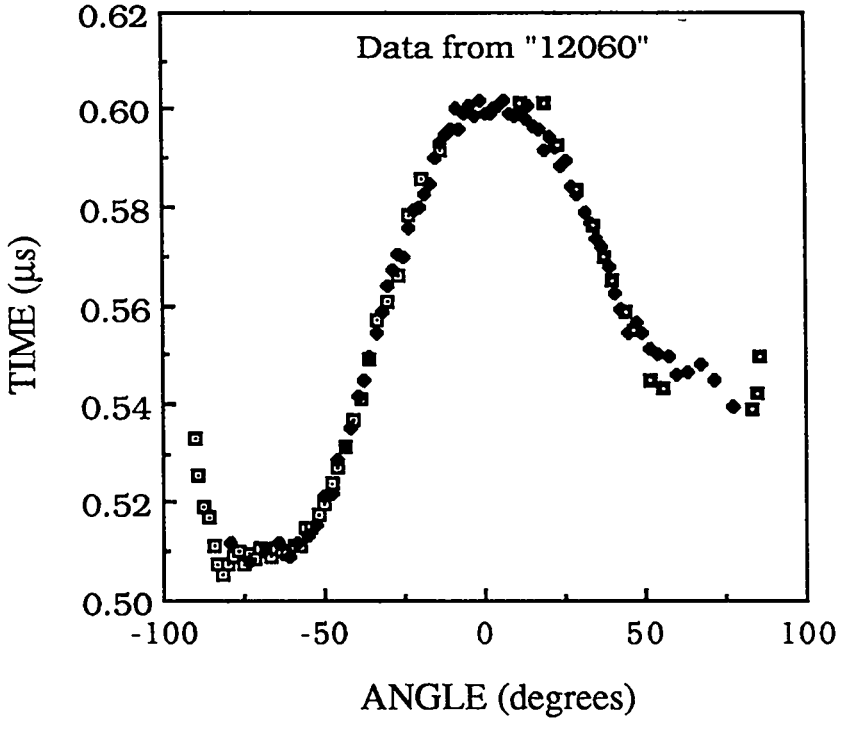
Data from "12060"
TIME (µs)
0.62
0.60
0.58
0.56
0.54
0.52
0.50
-100
-50
0
50
100
ANGLE (degrees)

A4

APPENDIX B

REDUCED VELOCITY-HISTORIES OF ALL THE VELOCIMETRY EXPERIMENTS

TABLE 1

TABLE OF THE JUMP VELOCITY AND ANGULAR LOCATION MEASURED FROM THE POLE OF THE HEMISPHERE FOR ALL THE EXPERIMENTS OF THIS STUDY

Figure Number	Shot Number	Jump Velocity (mm/μs)	Angle from Pole (degrees)
B1	F8077	2.95	48.3
B2	F8083	2.84	49.1
B3	F8091	2.95	0.98
B4	F8093	2.83	0.73
B5	F8094	2.96	63.98
B6	F8108	2.88	49.42
B7	F8109	3.06	36.6
B8	F8111	2.99	57.9
B9	F8126	2.98	44.2
B10	F8127	2.87	58.88
B11	F8128	2.92	47.75
B12	F8129	2.85	60.5
B13	F8130	2.85	42.75
B14	F1743	2.95	0.0
B15	F1744	2.85	0.0
B16	F1746	2.73	0.0
B17	F1747	3.05	0.0
B18	F1901	2.71	75.68
B19	F1902	2.95	64.1
B20	F1903	2.71	73.85

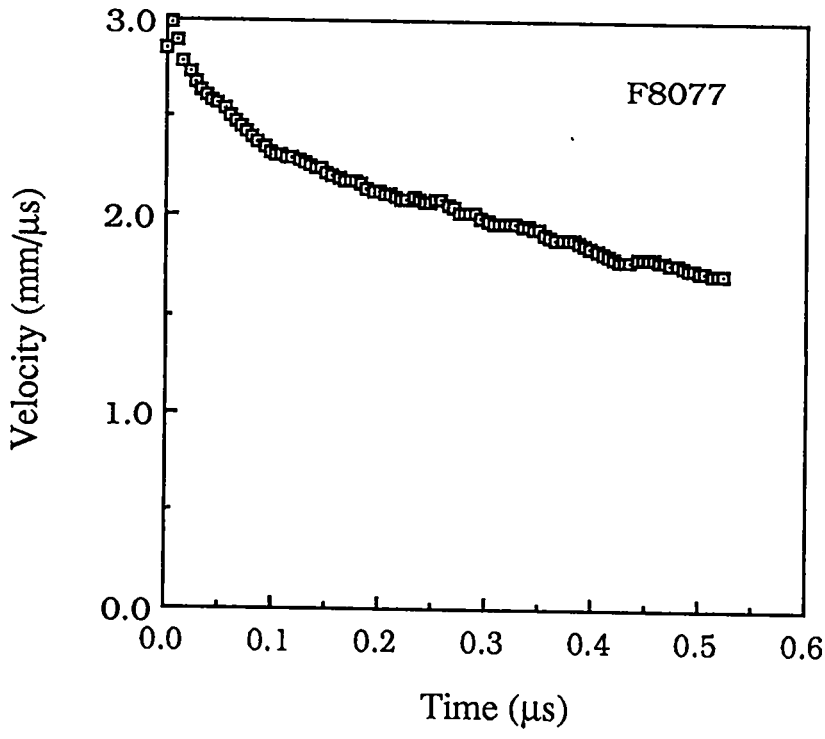
F8077
Velocity (mm/μs)
3.0
2.0
1.0
0.0
0.0
0.1
0.2
0.3
0.4
0.5
0.6
Time (μs)

B1

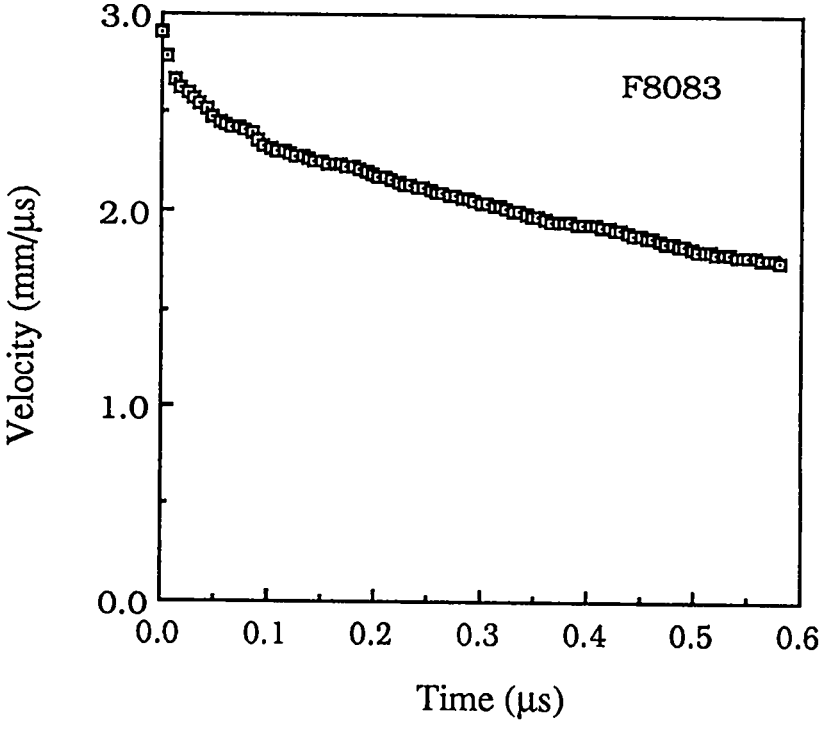
F8083
Velocity (mm/μs)
3.0
2.0
1.0
0.0
0.0
0.1
0.2
0.3
0.4
0.5
0.6
Time (μs)

B2

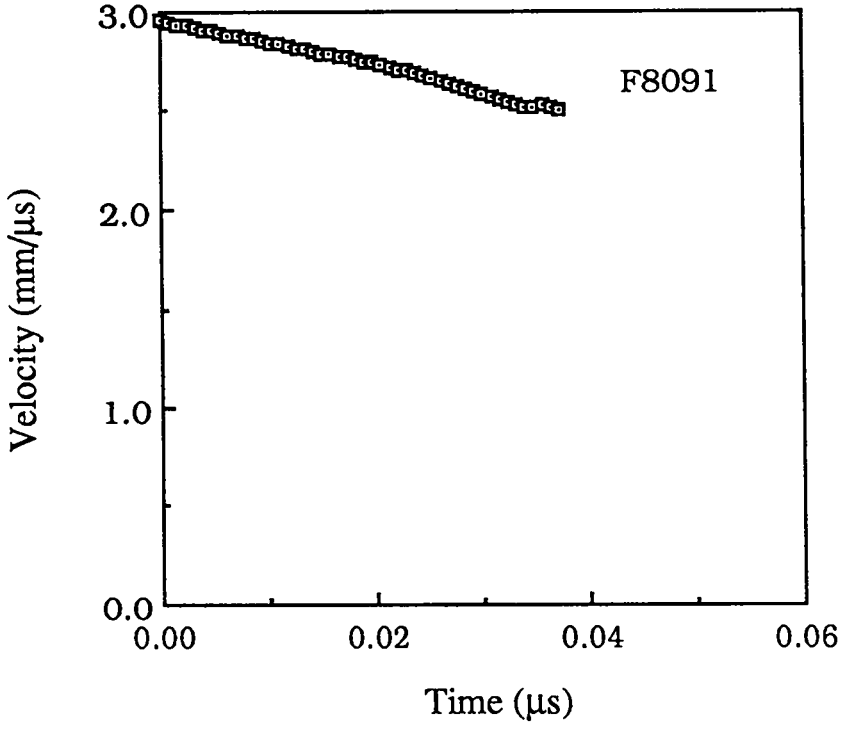
F8091
Velocity (mm/μs)
3.0
2.0
1.0
0.0
0.00
0.02
0.04
0.06
Time (μs)

B3

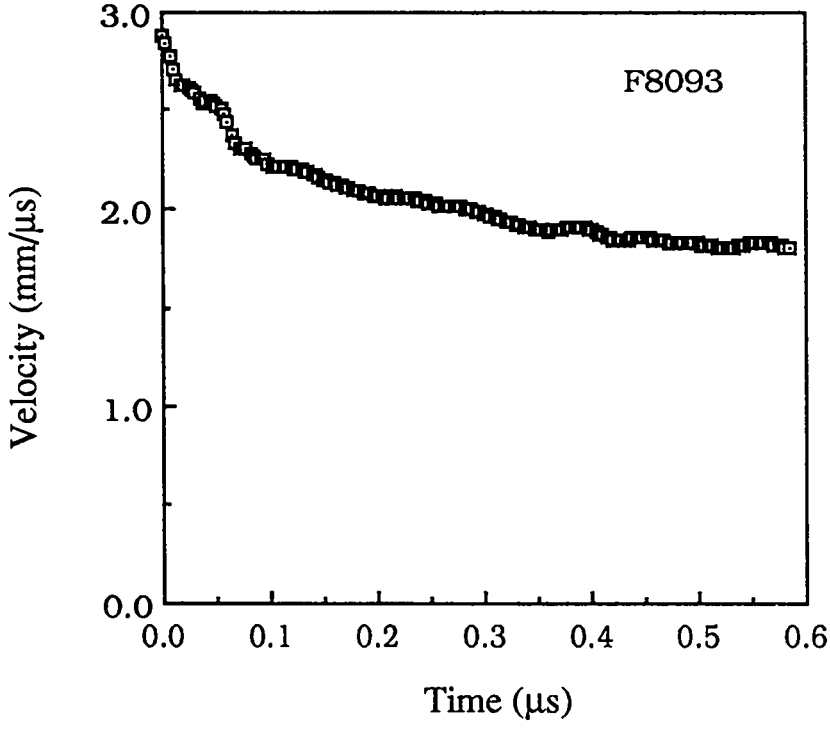
F8093
Velocity (mm/μs)
3.0
2.0
1.0
0.0
0.0
0.1
0.2
0.3
0.4
0.5
0.6
Time (μs)

B4

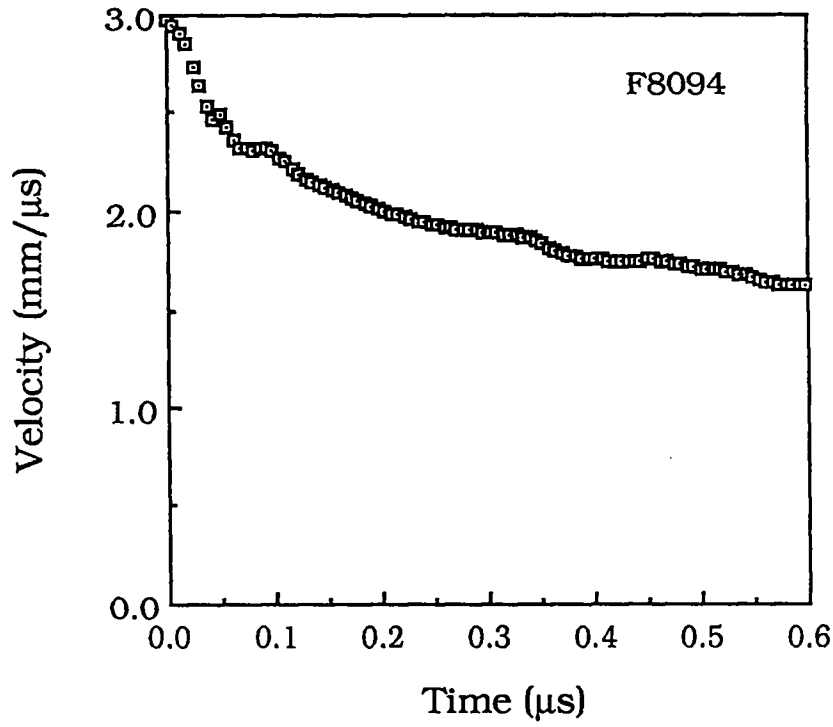
F8094
Velocity (mm/μs)
Time (μs)
3.0
2.0
1.0
0.0
0.0
0.1
0.2
0.3
0.4
0.5
0.6

B5

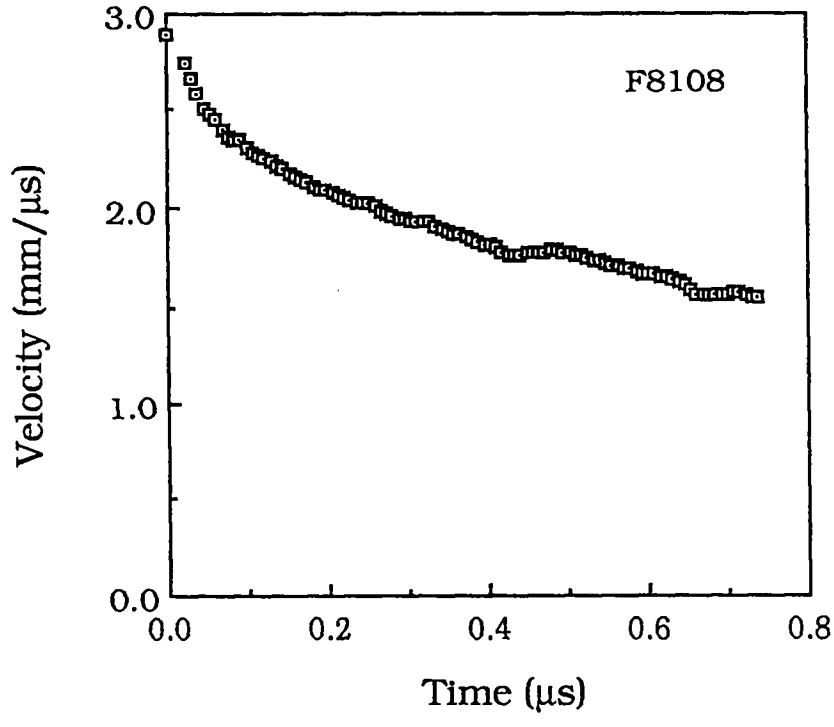
F8108
Velocity (mm/μs)
Time (μs)
3.0
2.0
1.0
0.0
0.0
0.2
0.4
0.6
0.8

B6

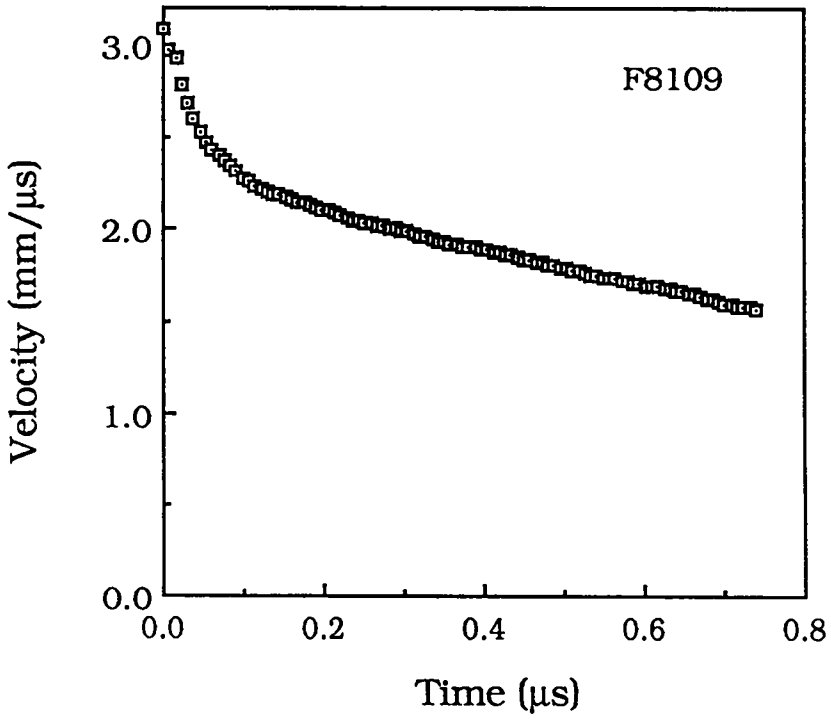
F8109
Velocity (mm/μs)
3.0
2.0
1.0
0.0
0.0
0.2
0.4
0.6
0.8
Time (μs)

B7

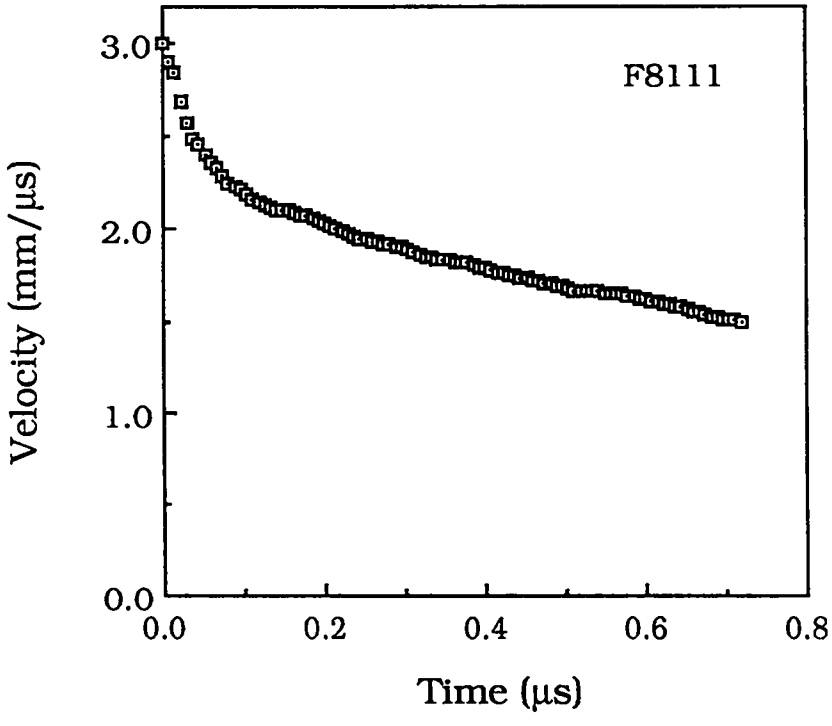
F8111
Velocity (mm/μs)
3.0
2.0
1.0
0.0
0.0
0.2
0.4
0.6
0.8
Time (μs)

B8

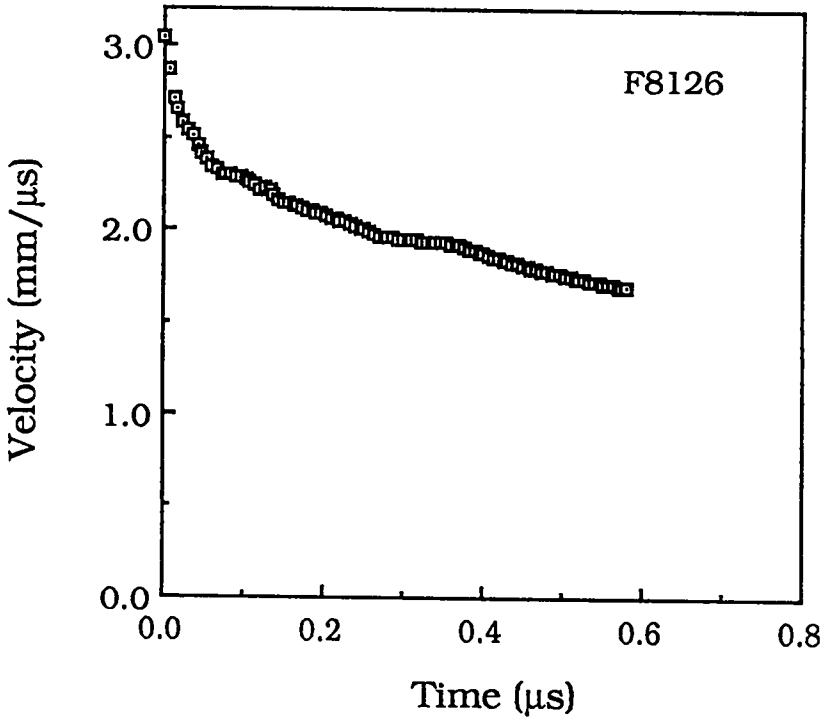
F8126
Velocity (mm/μs)
Time (μs)
3.0
2.0
1.0
0.0
0.0
0.2
0.4
0.6
0.8

B9

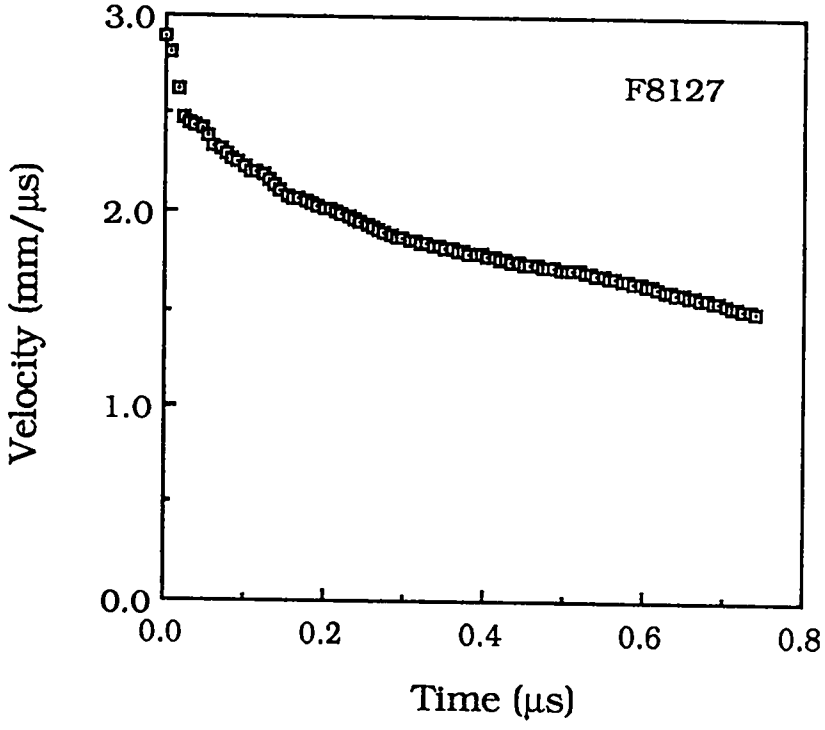
F8127
Velocity (mm/μs)
Time (μs)
3.0
2.0
1.0
0.0
0.0
0.2
0.4
0.6
0.8

B10

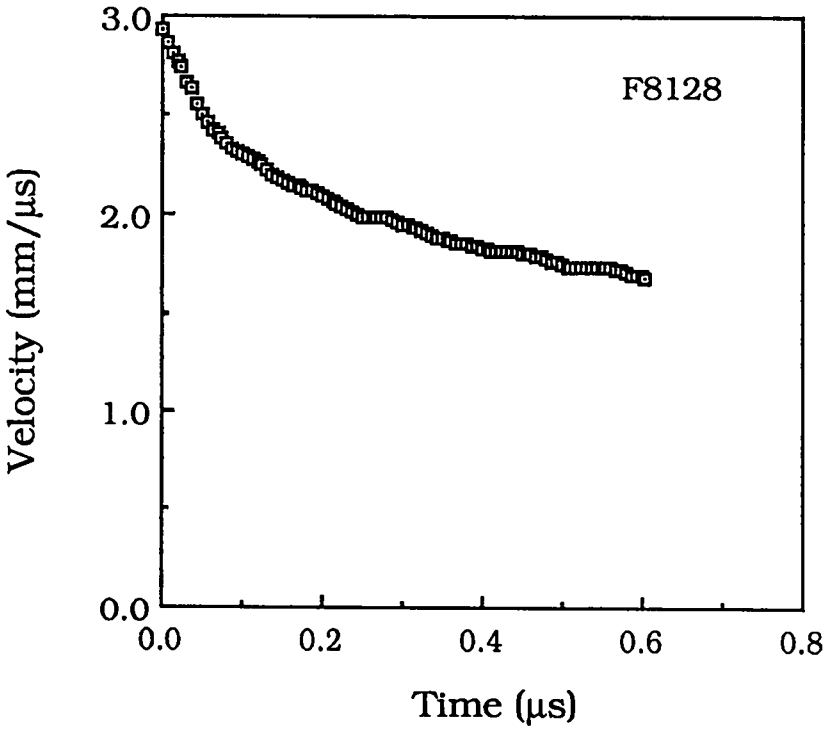
F8128
Velocity (mm/μs)
3.0
2.0
1.0
0.0
0.0
0.2
0.4
0.6
0.8
Time (μs)

B11

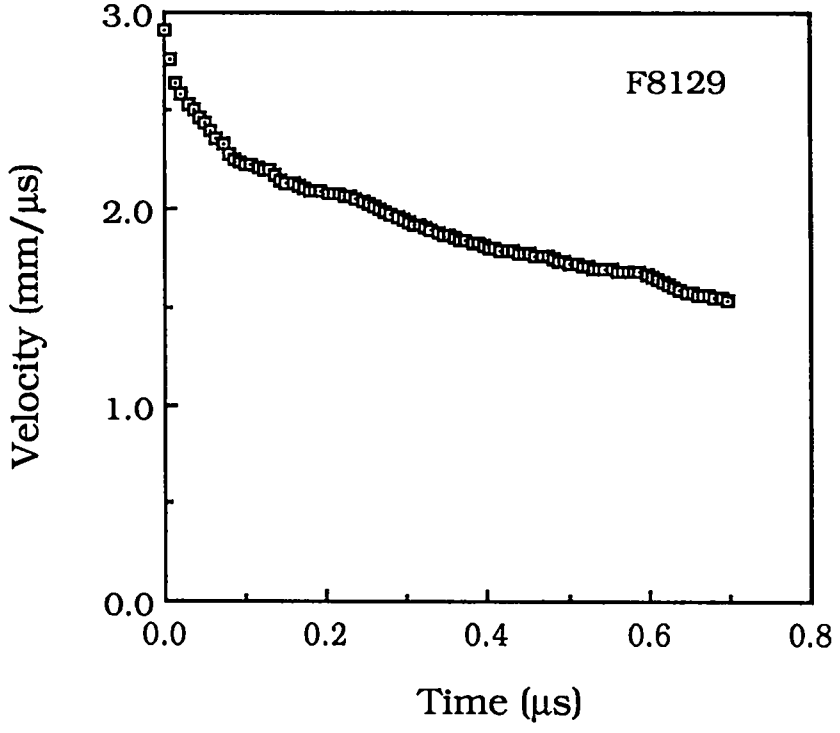
F8129
Velocity (mm/μs)
3.0
2.0
1.0
0.0
0.0
0.2
0.4
0.6
0.8
Time (μs)

B12

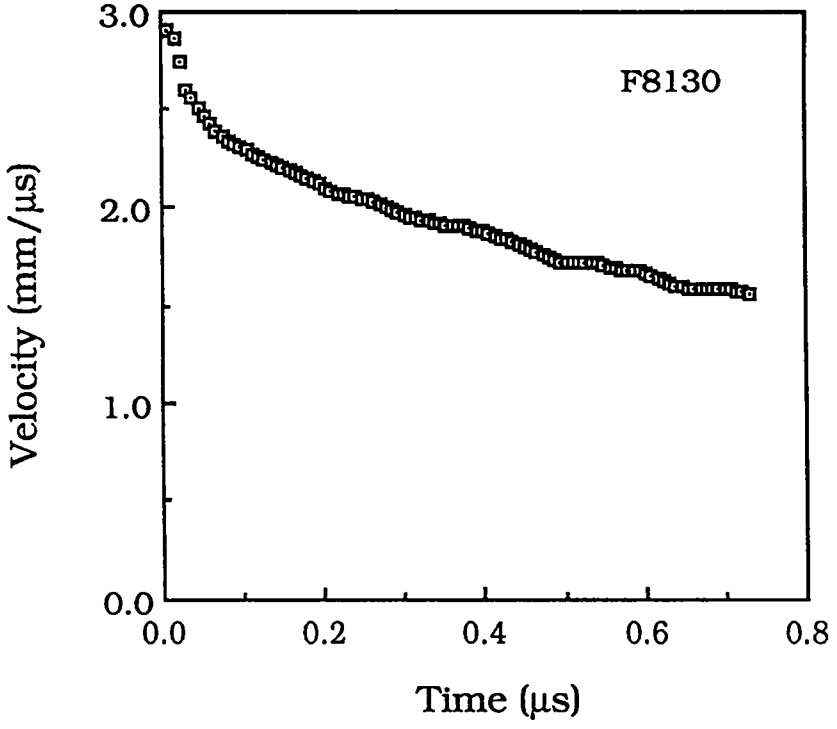
F8130
Velocity (mm/μs)
Time (μs)
3.0
2.0
1.0
0.0
0.0
0.2
0.4
0.6
0.8

B13

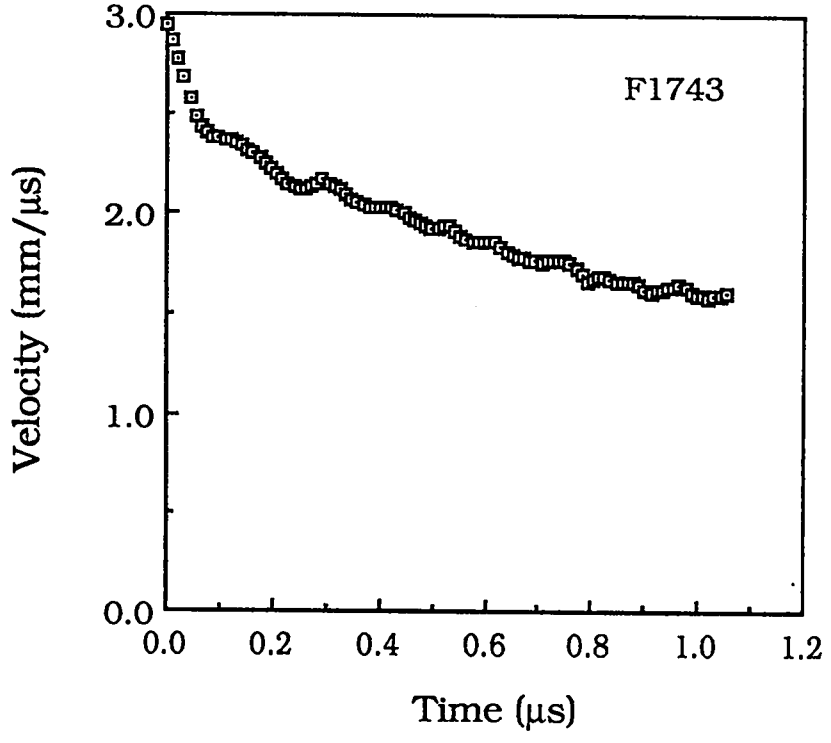
F1743
Velocity (mm/μs)
Time (μs)
3.0
2.0
1.0
0.0
0.0
0.2
0.4
0.6
0.8
1.0
1.2

B14

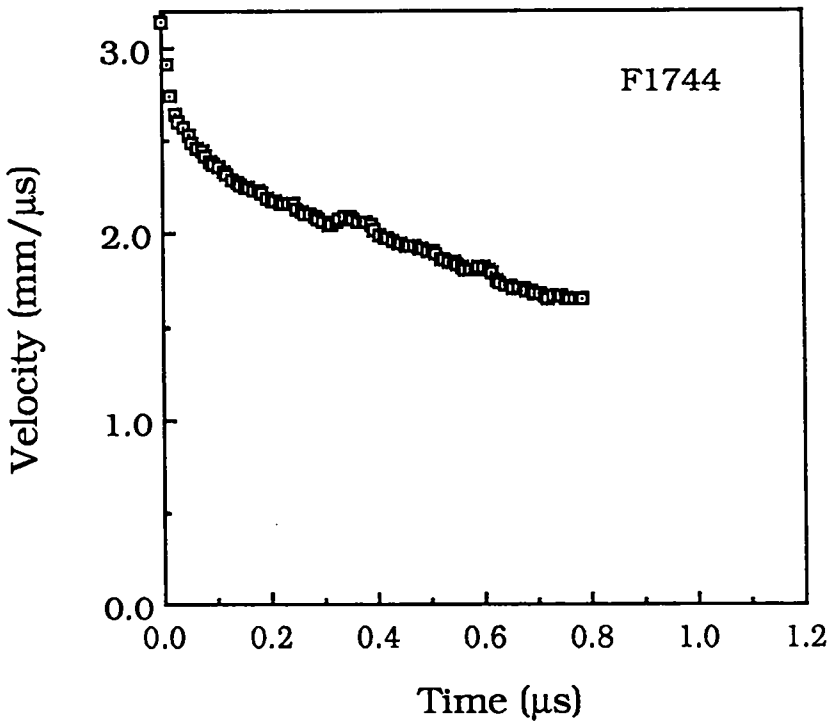
F1744
Velocity (mm/μs)
3.0
2.0
1.0
0.0
0.0
0.2
0.4
0.6
0.8
1.0
1.2
Time (μs)

B15

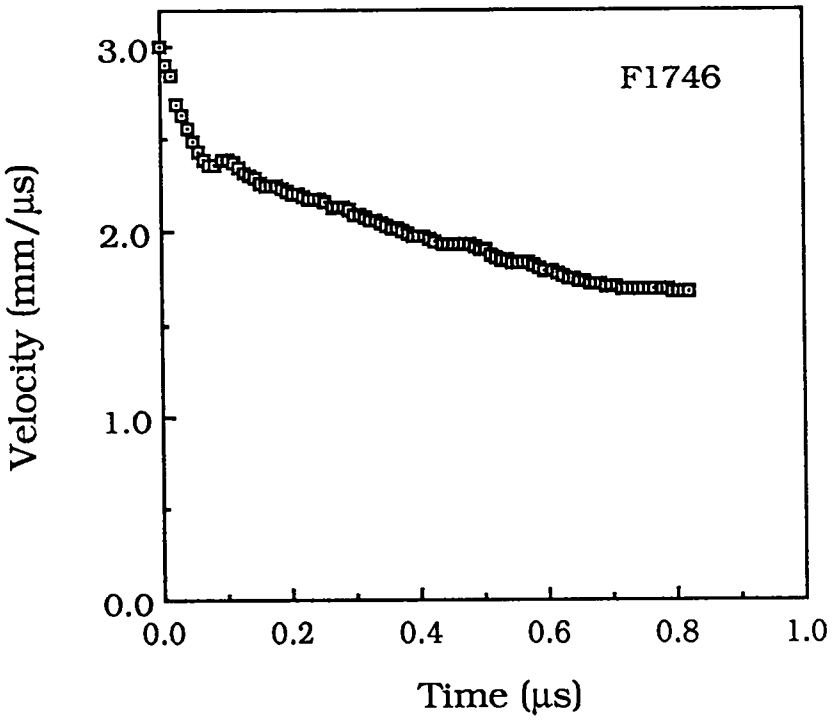
F1746
Velocity (mm/μs)
3.0
2.0
1.0
0.0
0.0
0.2
0.4
0.6
0.8
1.0
Time (μs)

B16

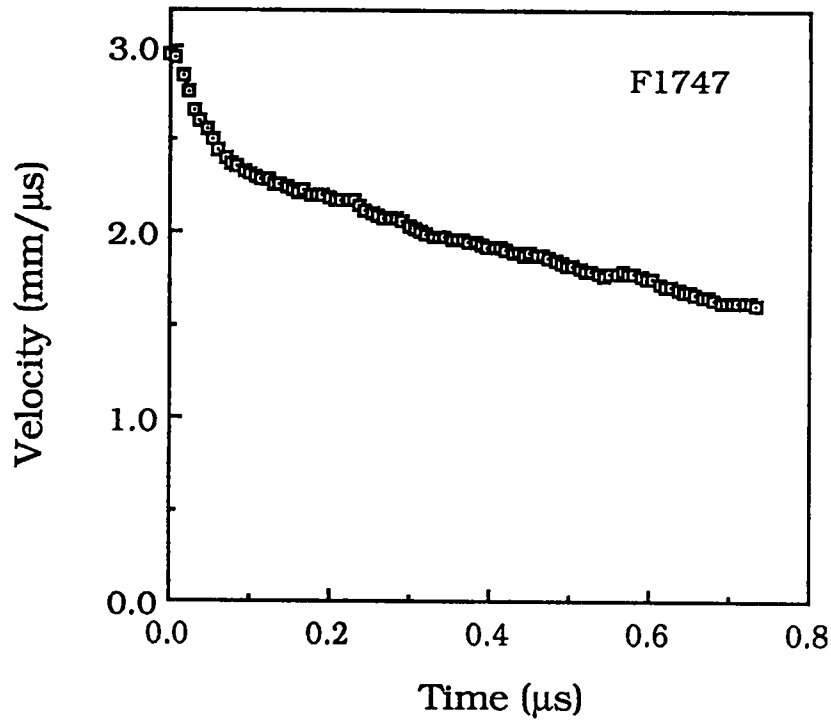
F1747
Velocity (mm/μs)
Time (μs)
3.0
2.0
1.0
0.0
0.0
0.2
0.4
0.6
0.8

B17

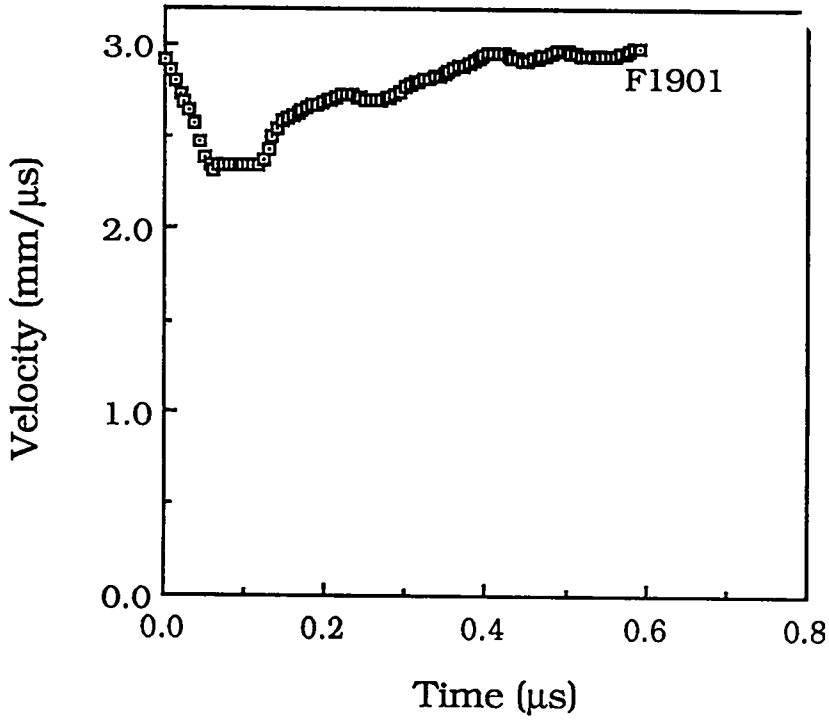
F1901
Velocity (mm/μs)
Time (μs)
3.0
2.0
1.0
0.0
0.0
0.2
0.4
0.6
0.8

B18

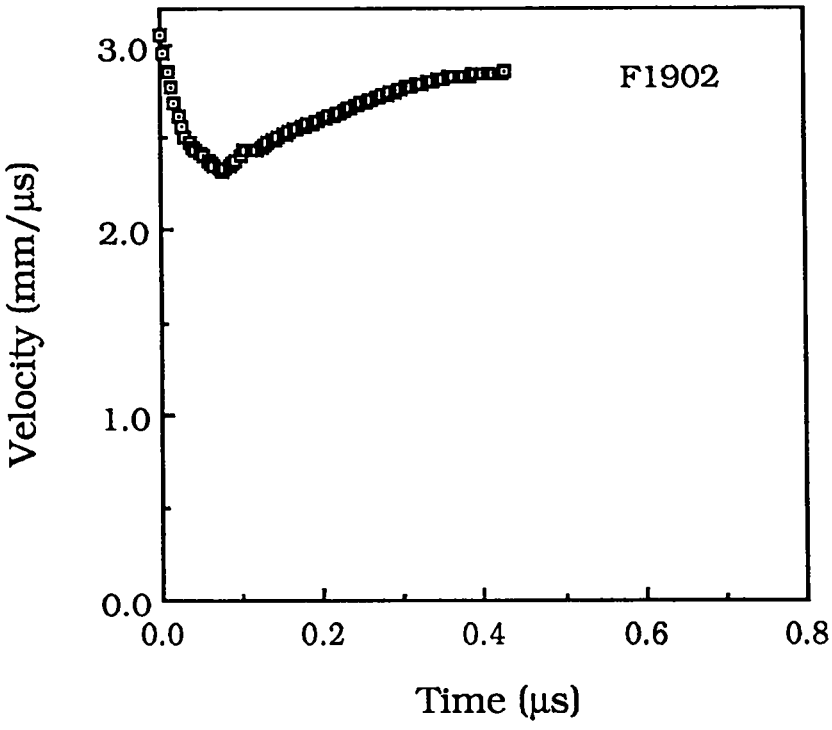
F1902
Velocity (mm/μs)
Time (μs)
3.0
2.0
1.0
0.0
0.0
0.2
0.4
0.6
0.8

B19

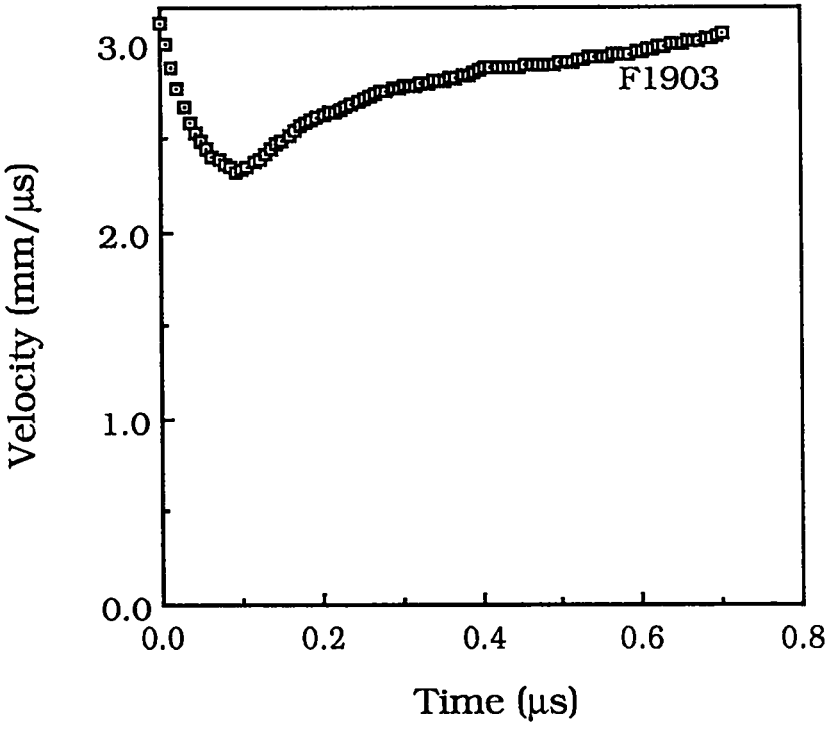
F1903
Velocity (mm/μs)
Time (μs)
3.0
2.0
1.0
0.0
0.0
0.2
0.4
0.6
0.8

B20

APPENDIX C

VELOCITY HISTORIES FOR THE SHOCK VELOCITY MEASUREMENTS IN THE PMMA WINDOW

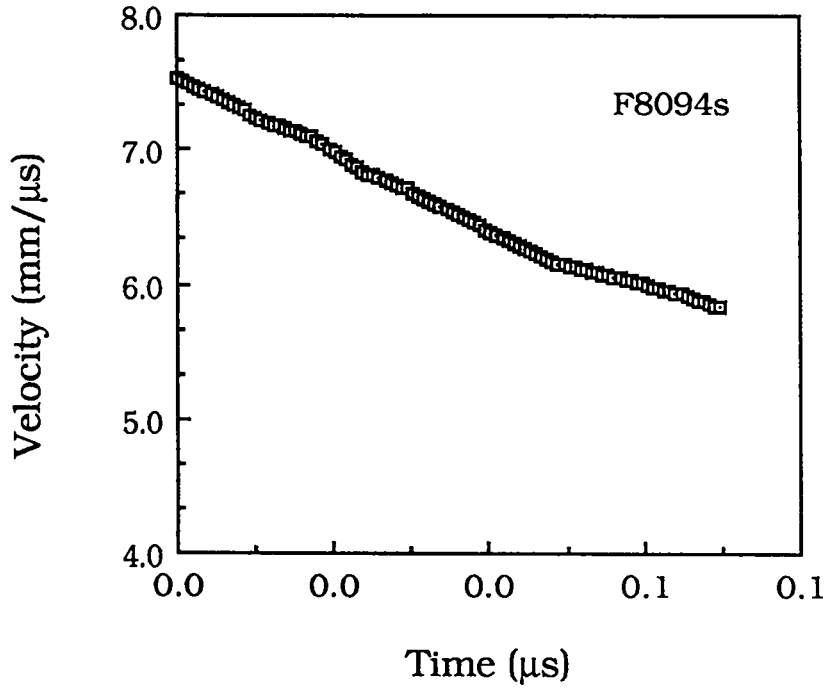
F8094s
8.0
7.0
6.0
5.0
4.0
Velocity (mm/μs)
0.0
0.0
0.0
0.1
0.1
Time (μs)

C1

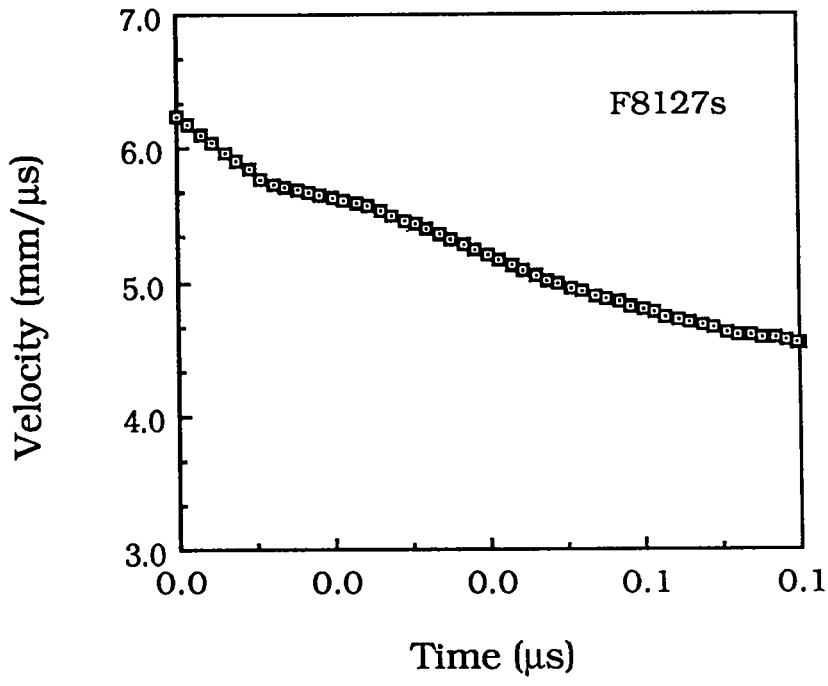
F8127s
7.0
6.0
5.0
4.0
3.0
Velocity (mm/μs)
0.0
0.0
0.0
0.1
0.1
Time (μs)

C2

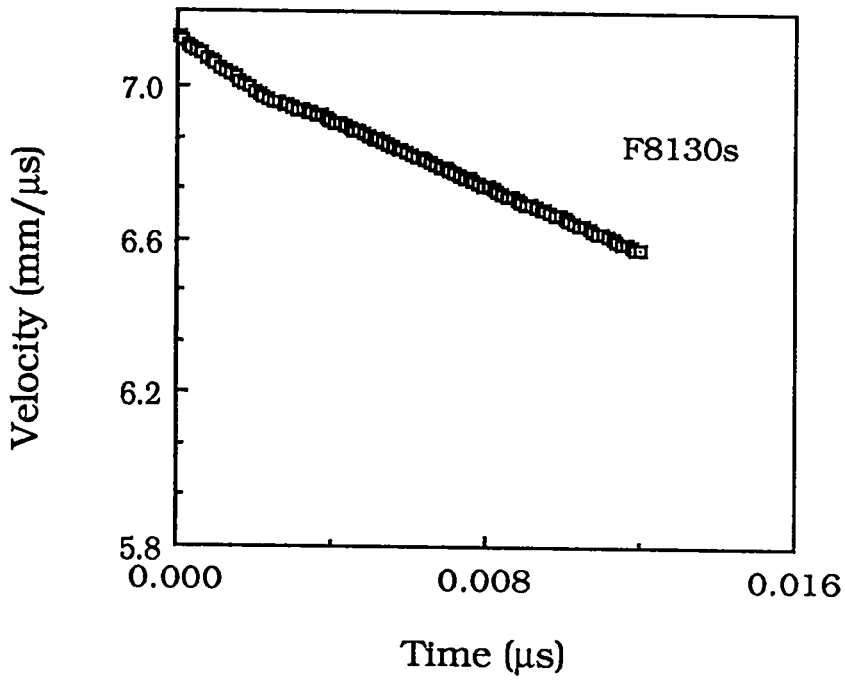
7.0
6.6
6.2
5.8
0.000
0.008
0.016
F8130s
Velocity (mm/μs)
Time (μs)

C3

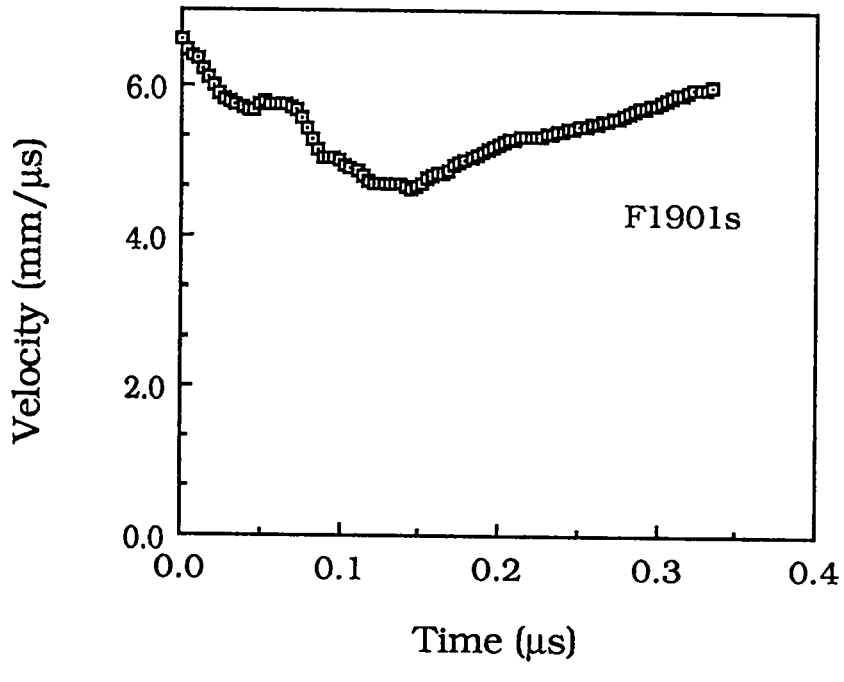
6.0
4.0
2.0
0.0
0.0
0.1
0.2
0.3
0.4
F1901s
Velocity (mm/μs)
Time (μs)

C4

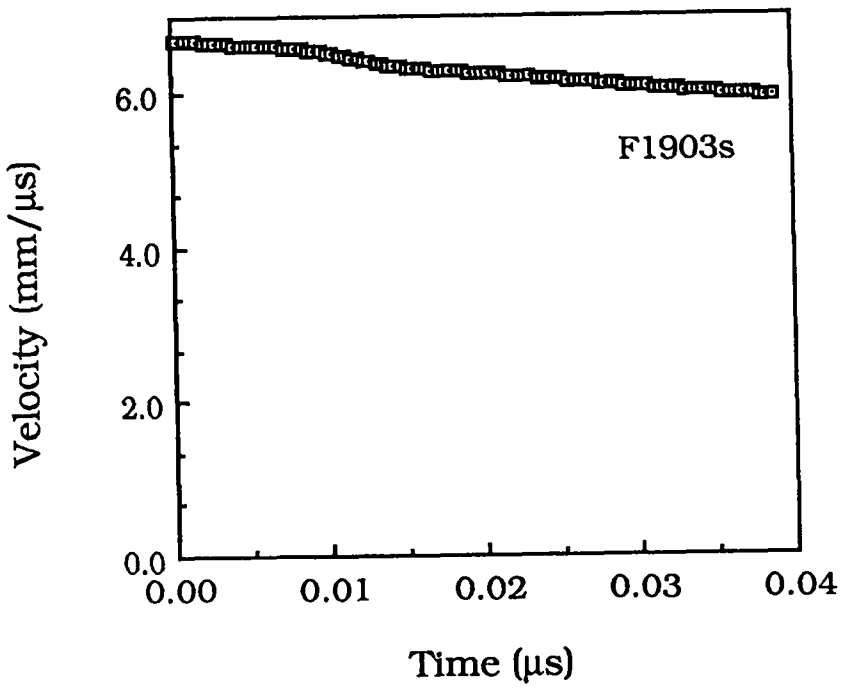

C5

Printed in the United States of America
Available from
National Technical Information Service
US Department of Commerce
5285 Port Royal Road
Springfield, VA 22161

Microfiche (A01)

Page Range	NTIS Price Code	Page Range	NTIS Price Code	Page Range	NTIS Price Code	Page Range	NTIS Price Code
001-025	A02	151-175	A08	301-325	A14	451-475	A20
026-050	A03	176-200	A09	326-350	A15	476-500	A21
051-075	A04	201-225	A10	351-375	A16	501-525	A22
076-100	A05	226-250	A11	376-400	A17	526-550	A23
101-125	A06	251-275	A12	401-425	A18	551-575	A24
126-150	A07	276-300	A13	426-450	A19	576-600	A25
						601-up*	A99

*Contact NTIS for a price quote.

Los Alamos National Laboratory
Los Alamos,New Mexico 87545